Drug Design, Development and Therapy

Dovepress
Taylor & Francis Group

Open Access Full Text Article

ORIGINAL RESEARCH

Network Pharmacology, Molecular Docking and Experimental Validation on Potential Application of Diabetic Wound Healing of *Cinnamomum zeylanicum* Through Matrix Metalloproteinases-8 And 9 (MMP-8 And MMP-9)

Sharmin Akter[1], Shihab Uddin Ahmad[1], Mohiuddin Ahmed Bhuiyan[1], Irin Dewan[1], Rumman Reza[2], Niaz Morshed[2], Md Nazmus Samdani[2], Md Selim Reza[2], Ajoy Kumer[3,4], Isa Naina Mohamed[5]

[1]Department of Pharmacy, School of Medicine, University of Asia Pacific, Dhaka, 1215, Bangladesh; [2]Department of Pharmaceutical Technology, Faculty of Pharmacy, University of Dhaka, Dhaka, 1000, Bangladesh; [3]Center for Global Health Research, Saveetha Medical College and Hospitals, Saveetha Institute of Medical and Technical Sciences, Chennai, TN, 602105, India; [4]Department of Chemistry, College of Arts and Sciences, International University of Business Agriculture and Technology, Dhaka, 1230, Bangladesh; [5]Department of Pharmacology, Faculty of Medicine, Universiti Kebangsaan Malaysia, Kuala Lumpur, 56000, Malaysia

Correspondence: Shihab Uddin Ahmad, Department of Pharmacy, School of Medicine, University of Asia Pacific, 74/A, Green Road, Dhaka, 1205, Bangladesh, Email shihab@uap-bd.edu; Isa Naina Mohamed, Department of Pharmacology, Faculty of Medicine, Universiti Kebangsaan Malaysia, Jalan Yaacob Latif, Bandar Tun Razak, Cheras, Kuala Lumpur, 56000, Malaysia, Email isanaina@ppukm.ukm.edu.my

Background: Diabetic wounds are a significant clinical challenge due to impaired healing processes often exacerbated by elevated matrix metalloproteinases (MMPs). *Cinnamomum zeylanicum*, known for its anti-inflammatory and antioxidant properties, has shown potential in promoting wound healing. This study investigates the molecular docking and experimental validation of *Cinnamomum zeylanicum*'s effects on diabetic wound healing, focusing on its interaction with matrix metalloproteinases-8 (MMP-8) and 9 (MMP-9).

Methods: Molecular docking studies were performed to predict the binding affinity of *Cinnamomum zeylanicum* compounds to MMP-8 and MMP-9. Diabetic wound healing was evaluated using in vivo models where wounds were induced and treated with *Cinnamomum zeylanicum* extract. Various parameters were measured, including wound contraction, hydroxyproline content, superoxide dismutase (SOD), catalase (CAT), glutathione peroxidase (GPx), and malondialdehyde (MDA) levels. Biochemical analyses included glucose levels, fasting blood glucose (FBG), oral glucose tolerance test (OGTT), and histomorphological examination of skin tissues.

Results: Molecular docking results indicated a high binding affinity of *Cinnamomum zeylanicum's* bioactive compounds with MMP-8 and MMP-9, suggesting potential inhibition. Experimental validation showed significant improvement in wound contraction and increased hydroxyproline content, indicating enhanced collagen synthesis. Antioxidant enzyme activities (SOD, GPx, CAT) were significantly elevated, while MDA levels were reduced, reflecting decreased oxidative stress. Biochemical analysis demonstrated improved glucose homeostasis with reduced FBG and enhanced OGTT responses. Histomorphological studies revealed improved tissue architecture and re-epithelialization in treated wounds.

Conclusion: *Cinnamomum zeylanicum* exhibits promising potential in diabetic wound healing by modulating MMP-8 and MMP-9 activities, enhancing antioxidant defenses, and improving glucose regulation. These findings support its therapeutic application for diabetic wounds, providing a foundation for further clinical investigations.

Keywords: *Cinnamomum zeylanicum*, xanthosine, methylquinoline, matrix metalloproteinase, wound healing

Received: 4 October 2024
Accepted: 8 February 2025
Published: 12 March 2025

Introduction

Diabetic wounds represent a significant clinical challenge due to the complex interplay of various pathological factors that impair the normal wound healing process.[1,2] These wounds commonly occur in individuals with diabetes mellitus, where prolonged hyperglycemia leads to microvascular complications, neuropathy, and immune dysfunction, collectively contributing to impaired wound healing.[3–5] The hallmark features of diabetic wounds include delayed inflammation, aberrant angiogenesis, impaired collagen deposition, and increased susceptibility to infections, culminating in chronic non-healing ulcers.[6,7] Current treatment modalities for diabetic wounds primarily focus on managing underlying risk factors such as glycemic control, infection control, and offloading pressure from the wound site.[8] Standard wound care practices encompass debridement, wound cleansing, dressings, and offloading techniques, aimed at promoting a conducive environment for healing.[9] Despite these interventions, diabetic wounds often exhibit poor response rates and high recurrence rates, highlighting the urgent need for novel therapeutic approaches. Emerging strategies in diabetic wound management include the utilization of natural products with anti-inflammatory, antioxidant, and proangiogenic properties, which holds promise in promoting wound healing through modulation of different molecular targets.[10] Integrating such innovative therapies with conventional approaches may offer a multifaceted approach to enhance the healing outcomes of diabetic wounds and alleviate the considerable burden associated with this debilitating complication of diabetes.[11]

Cinnamomum zeylanicum (CZ), an ancient herbal remedy dating back four thousand years, has gained recognition for its therapeutic properties.[12,13] CZ demonstrates diverse health benefits, including antimicrobial, anti-inflammatory, and blood glucose-regulating properties, along with potential cardiovascular and cognitive benefits, and cancer risk reduction.[14–16] In vitro experiments have highlighted CZ's antioxidant potential, enhancing antioxidant enzyme activity and exhibiting antibacterial effects against *Escherichia coli, Pseudomonas aeruginosa*, and *Staphylococcus aureus*.[17,18] CZ has long been investigated as a potential treatment for type 2 diabetes, revealing insulin-potentiating properties in vivo and in vitro studies.[19] Notably, aqueous extracts of CZ have been found to enhance glucose metabolism and insulin action.[20]

The ability of CZ to cure wounds was addressed in numerous recently published papers, but none specifically addressed cinnamon's ability to heal wounds in diabetic conditions. In addition, understanding the intricate interactions between bioactive components of cinnamon and their molecular targets is crucial for elucidating its therapeutic potential in managing diabetic wounds. In addition, precise molecular mechanisms through which CZ exerts its therapeutic effects on diabetic wound healing remain unknown. In recent years, network pharmacology and molecular docking have emerged as powerful tools in drug discovery and development, facilitating the identification of potential molecular targets and elucidation of drug-target interactions.[21,22] By integrating network pharmacology and molecular docking analyses, comprehensive insights into the pharmacological mechanisms of natural compounds such as cinnamon can be obtained, aiding in the rational design of novel therapeutic strategies for diabetic wound healing.[23] Purpose of the study is to employ a systematic approach combining network pharmacology and molecular docking analyses to investigate the interactions between bioactive constituents of CZ and molecular targets, particularly MMP-8 and MMP-9 proteins implicated in wound healing processes, thereby shedding light on its therapeutic potential in the management of diabetic wounds.

Materials and Methods

Plant Extraction Process and Phytochemical Identification

The CZ bark was purchased from a local market and authenticated by the Department of Plant Taxonomic Research and Museum, Bangladesh National Herbarium (BNH), Ministry of Environment, Forest and Climate Change and deposited at the BNH as specimen No. DACB 91376. The extract was prepared through a cold extraction method using ethanol. Briefly, around 4 kilograms of CZ bark were dried, cut into small pieces, and submerged in 20 liters of ethanol for 15 days. Afterwards, it was filtered using a cotton filtration process, and the filtrate was collected until it became a clear, colorless liquid. The filtrate was then concentrated using a rotary evaporator to produce the ethanolic extract of CZ, which was later stored at a temperature of 4 °C until use.

The gas chromatography-mass spectrometry (GC-MS) analysis was performed using a Clarus® 690 gas chromatograph (PerkinElmer, CA, USA) and a column (Elite-35, 30 m × 0.25 mm; PerkinElmer, CA, USA) with a 0.25 µm film. Additionally, the gas chromatograph was equipped with a Clarus® SQ 8 C mass spectrometer (PerkinElmer, CA, USA). A 1 µL sample was injected (splitless mode), and helium with a purity of 99.999% was utilized as the carrier gas at a constant flow rate of 1 mL/min for 40 minutes. The sample was evaluated in high-energy EI (electron ionization) mode (70 eV). Although the inlet temperature remained unchanged at 280 °C, the column oven temperature was initially set at 60 °C (for 0 minutes), increased at a rate of 5 °C per minute to 240 °C, and maintained for 4 minutes. The scan period was 1 second, and the mass range was 50–600 m/z. Sample chemicals were identified by comparing them to the National Institute of Standards and Technology (NIST) database.

In Silico Assessment

Assessment of Disease-Gene Association

One of the largest publicly available datasets of genes and variations linked to human disorders may be found on the platform called DisGeNET.[24] DisGeNET web-server was used in the current study to investigate the association between diabetic wound healing and matrix metalloproteinase proteins (MMP8 and MMP9). In the search section of the web tool, "diabetic wound healing" was used as a keyword. The summary of the disease was generated using the default search parameters. In the disease-gene association summary sub-section, several genes associated with diabetic wound healing were tabulated with relevant information such as disease specificity index, disease pleiotropy index, gene-disease association score, and the probability of being loss-of-function intolerant.

Protein-Protein Network Analysis

STRING is a biological repository and online resource for known and anticipated protein–protein interactions in molecular biology.[25] The STRING platform was used to build a protein–protein interaction network for MMP-8 and MMP-9. In the designated search field of the web tool, the target protein was entered as input. The intended organism was set to Homo sapiens for the search results. The web tool generated a network of proteins in the form of colored nodes, showing the first line of interacting proteins with the target proteins.

Investigation of Association Between Disease and Gene Expression

Enrichr is a bioinformatics tool that can be utilized to investigate different pathways in which a gene and its co-expressed genes are involved.[26] Enrichr web-server was used in this research to analyze the association between diseases such as microvascular complications of diabetes and diabetic perturbations with target protein alongside its co-expressed genes. At first the web-server generated a database of MMP8 and 100 co-expressed genes utilizing default settings and algorithm. The following parameter was set for co-expressed gene database creation: Top 100 genes co-express with MMP8 identified with ARCHS4 RNA-seq gene–gene co-expression. The database was further used for analysis purposes. After the search operation was over, the web-server showed various sources of information for disease-gene association. ClinVar 2019 and diabetic perturbation GEO 2022 archives were used in the current study.

Molecular Docking Studies

For macromolecular structures to be more accessible, macromolecular protein processing is necessary. Atomic collisions can be eliminated, hydrogen bonds can be added and optimized, connected water molecules can be removed, and other procedures necessary for docking investigations can be carried out using refinement techniques. For the current investigation, the experimentally verified electron microscopy structures of MMP8 and MMP9 proteins were taken from the protein data repository. Then, in order to clean and refine these protein structures, the BIOVIA Discovery Studio 2020 Client was used. Water molecules were removed, followed by the elimination of cofactors, mineral ions, and other heteroatoms.

The ligands' structure data files (SDF) were obtained from the PubChem database. The PubChem database was used to collate the Structure Data Files for every ligand. Using PyRx software, the files were opened, and each ligand SDF was copied to the Open Babel area. The Open Babel platform was used for ligand optimization, which involved minimizing the ligands and converting them to pdbqt format.

PyRx was used to carry out molecular docking in the following phase. One well-known virtual screening tool that has been used to identify multiple potential treatment candidates is PyRx. PyRx uses score-based Lamarckian Genetic Algorithms (LGAs), specifically AutoDock and AutoDock Vina. AutoDock Vina was used to perform independent docking with each of the compounds after accessing the PDB files of the target protein that were thus created. After the compounds were eventually docked, the target protein macromolecule was visualized using the BIOVIA Discovery Studio Visualizer Software, revealing the binding interactions with specific ligands.

Interaction Studies of Ligand-Protein Docked Complexes

The interacting bonds that the ligands make with the target macromolecular protein structure were investigated by generating two-dimensional (2D) interaction diagrams in Discovery Studio software. First, the protein-ligand docked complexes for the top ligands with high binding affinities were generated in protein data bank (PDB) file format using PyMOL software. After this, the PDB format files were each opened separately in Discovery Studio, where the ligand-protein interactions were visualized.

ADMET Prediction

The SwissADME web-server was used to predict the Absorption, Distribution, Metabolism and Excretion profiles of all the ligands.[27] SwissADME webserver was used to assess whether natural substances were drug-like. The following criteria were used: BBB permeant, ESOL Class, number of Lipinski rule violations, GI absorption, CYP inhibitor, and bioavailability grade. The ligand structure data files were gathered from PubChem. The files that were downloaded were uploaded one after the other to the webservers of SwissADME. The retrieved data were tabulated in Microsoft Excel.

Biological Activity Estimation

PASS (Prediction of Activity Spectra for Substances) Online predicts more than 4000 different types of biological activity, such as effects on metabolism and transporters, pharmacological implications, biological mechanisms of action, toxic and detrimental impacts, and influence on gene expression.[28] PASS ONLINE is a subsidiary section supported by way2drug web-server. PASS ONLINE simultaneously predicts many distinct types of biological activity based on the structure of chemical substances. Prior to chemical synthesis and biological testing, PASS can be used to forecast the biological activity profiles for simulated molecules. Our top-recommended compounds' anti-microbial properties were predicted using the PASS online web server. Within the web server's designated search box, the canonical SMILES of the compounds with good binding affinities and ADMET parameters were integrated. The biological activity is defined by Pa (probability of activity) score. The activities with highest Pa scores were recorded and tabulated in MS Excel with the threshold level set at 0.80.

Molecular Dynamics Simulation

Dynamics simulation is a dependable and valuable tool in the study of biomolecules and experimental methods.[29] Energy minimization is a crucial preparatory step in molecular dynamics (MD) simulations, designed to optimize the system's geometry and eliminate unfavorable interactions that could lead to artifacts during the simulation. The process begins with applying the steepest descent algorithm, which is effective for quickly reducing large gradients in the potential energy landscape. This method ensures that high-energy steric clashes or overlaps between atoms are resolved in the initial stages. For instance, ligand-docking applications typically use this simulation technique to look at conformational space. Moreover, the interaction of two biological molecules like protein-drug interactions or protein–protein interactions can be studied by using molecular docking and molecular dynamics will provide us with a better understanding of what will happen to these interacting molecules over time.

Normal mode analysis (NMA) dynamics simulation was conducted using the iMODS server (https://imods.iqfr.csic.es/).[30] This approach allowed for the exploration of the flexibility and conformational changes in the protein-ligand complex, thereby validating the stability and accuracy of the docking results. By utilizing NMA, the simulation provided valuable information on the possible movements and stability of the biomolecular structures, enhancing our understanding of their interactions and potential efficacy.

In Vivo Experimental Assessment

Ointment Preparation

Lanolin, white soft paraffin, and liquid paraffin were used to make an emulsifying ointment to be used as a vehicle for topical preparation. The ingredients were put together on a clean glass plate and mixed using a spatula until a whitish-soft semisolid consistency formed. A 2% CZ ointment was prepared using the weighed amount of CZ extract and ointment base. Dose has been optimized by previous study.[31] The ingredients were combined homogeneously using a spatula and a glass plate and stored in a tightly sealed jar with proper labels.

Excision Wound Model and Treatment

Ninety Wistar rats were collected from the Animal Research Center of Jahangirnagor University. All rats weighed 150–200 g and 3 to 4 months old. The animals were acclimatized for one week to a laboratory setting that included temperatures of 22 ± 5 °C, 80 ± 10% humidity, and 12-hour day/night cycles. They were provided with food pellets and water on an *ad libitum* basis. The rats were equally distributed into five groups: non-diabetic sham control (SC), diabetic negative control without treatment (NC), diabetic vehicle control (VC), diabetic group treated with povidone-iodine as standard treatment (ST) and diabetic group treated group with CZ extract (CE). Each group contained eighteen rats, with six used for wound contraction measurement and six for histological and biochemical analysis on days 3 and 9. Each dataset was treated as a separate, independent measurement.

Four experimental groups (NC, VC, ST and CE) were induced severe diabetes conditions by administering alloxan monohydrate (SISCO Research Lab) intraperitoneal injection (120 mg/kg body weight) for three days.[32] Fasting blood glucose (FBG) and oral glucose tolerance test (OGTT) levels were recorded after 72 hours using glucometer (Onetouch Ultra, China) to assess the diabetes condition of rats. Rats with diabetic condition were chosen for investigating of wound healing effect based on a conventional criterion (FBG > 10 mmol/L).

The wound-healing effect was investigated using an excision wound model.[33] Rats were weighed and anesthetized with ketamine hydrochloride (50 mg/mL) before their dorsal hair was clipped. Four wounds were created on each rat's dorsal skin using an 8 mm biopsy punch and measure wound surface diameter by caliper. The non-diabetic sham control (SC) and diabetic control (NC) groups did not receive any treatment, while the other groups (VC, ST and CE) were treated with ointment base, povidone-iodine and CZ extract ointment respectively. Daily open wound dressing was performed until complete healing.

Wound Contraction Measurement

Two criteria such as macroscopic appearance and wound surface area were set to evaluate the wound contraction during healing process. Photos of wound area were taken with a digital camera and wound size was measured using a digital caliper with clock approach.[33,34] Wound size and photographs were taken on day 0 (zero), 3, 6, 9, 10 and followed until healing was complete. Determination of "complete healed day" based on the assessment of duration of wounds across individual rats, subsequently averaging the results for six rats per group.

Immunoassay

Wound tissue samples measuring 1.0 cm × 1.0 cm were excised on day 3 and day 9 post-wounding for immunoassay of protein levels, endogenous antioxidant enzyme and lipid peroxidation activities. Each tissue sample was dried, weighed, and transferred to an Eppendorf tube containing digestion buffer solution. The samples were homogenized using a microtube homogenizer (Benchmark Scientific, USA) and subsequently centrifuged at 8000 g for 10 minutes at 4°C to remove insoluble materials, and take the supernatant on ice before testing. The supernatant was collected for further biochemical estimations, which included the immunoassay of hydroxyproline content, superoxide dismutase (SOD), catalase (Cat), glutathione peroxidase (GPx), and malondialdehyde (MDA) levels. All assay kits were purchased from Solarbio, China, and analyzed according to manufacturer's protocols.

Histomorphological Analysis

On days 3 and 9, skin tissue was collected and fixed in 10% neutral-buffered formalin, then processed through a series of alcohol solutions with decreasing concentrations, rinsed with xylene, infiltrated with tissue, and embedded in paraffin

wax. Tissue sections were cut perpendicularly to the wound, dewaxed with xylene, and stained with hematoxylin and eosin (H & E) for general morphological assessment. These stained skin slides were examined under a light microscope, and images were captured for further analysis. Stained samples were evaluated by histology experts blindly using a modified numerical scale ranging from 0 to 3 (Table S1).

Statistical Analysis

The Statistical Package for the Social Sciences was used to analyze all quantitative data as means with standard errors of the mean (SEM) (SPSS, version 23.0). One-way ANOVA with Tukey's HSD post-hoc test determined significant differences. If $p < 0.05$, it was significant.

Results and Discussion

Phytochemical Profiling of CZ

In GC-MS analysis, 33 compounds were identified from the experimental extract. Figure 1 represents the distinct GC-MS chromatogram.

The bioactive compounds were represented by their retention time (RT), chemical formula, molecular weight and peak area in Table 1. Major compounds were detected cinnamaldehyde (10.88%), eugenol (10.19%), xanthosine (9.10%), α-pinene (5.78), quinoline (5.29%) and quinoline derivatives like methylquinoline (4.97%).

Disease-Gene Association and Network Pharmacology Studies

The DisGeNET web-server incorporates information from scholarly literature, animal models, GWAS libraries, and expert-curated sources. DisGeNET data are uniformly labelled using community-driven ontologies and controlled vocabularies. Furthermore, a number of unique indicators are offered to help prioritize the links between genotype and phenotype. DisGeNET (v7.0) currently includes 369,554 variant-disease associations (VDAs) between 194,515 variants and 14,155 diseases, traits, and phenotypes, and 1,134,942 gene-disease associations (GDAs), between 21,671 genes and 30,170 diseases, disorders, traits, and clinical or abnormal human phenotypes.

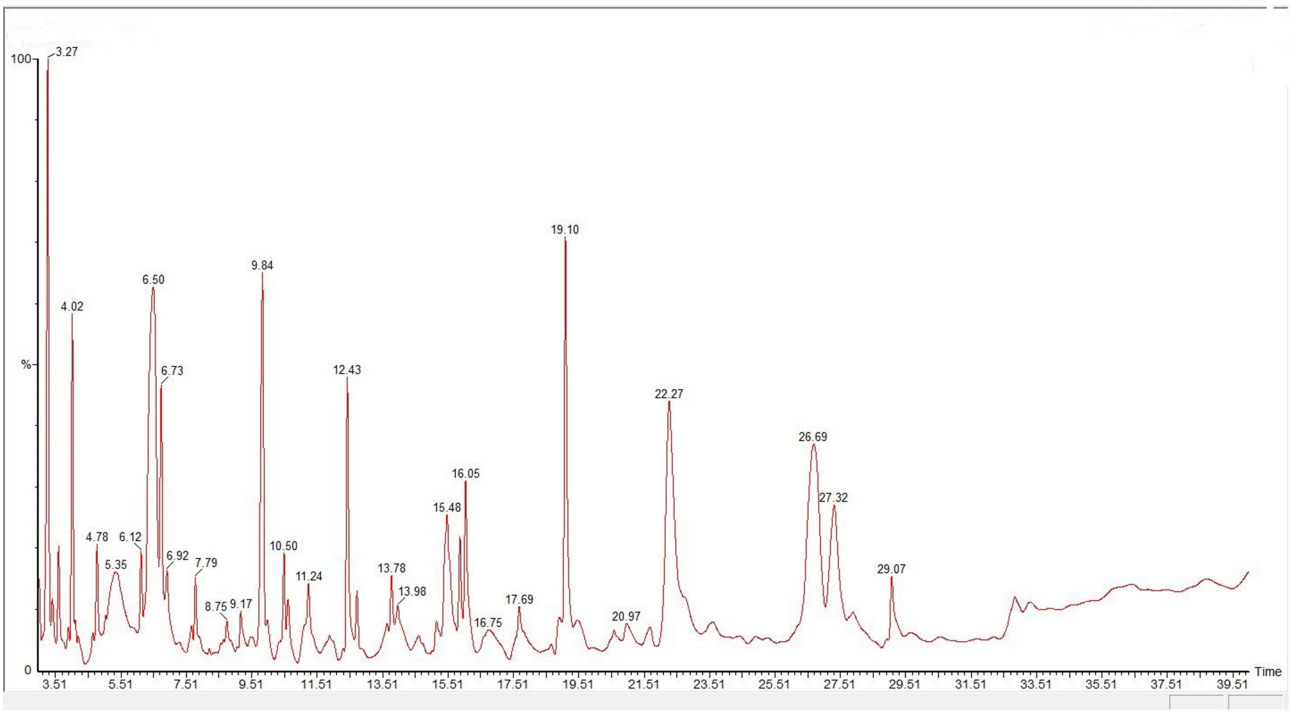

Figure 1 Gas Chromatography mass spectroscopic (GC-MS) base chromatogram of CZ bark ethanol extract.

Table 1 Gas Chromatography-Mass Spectroscopic Data of Compounds in CZ Bark Extract

Serial No.	Retention Time	Compounds Name	Chemical Formula	Molecular Weight (g/mol)	Peak Area (%)
1	3.27	Inositol	C6H12O6	180	4.66
2	3.60	Cyclobutanethiol	C4H8S	88	0.59
3	4.02	Glycine	C2H5NO2	75	2.82
4	4.78	Imidazole-4-methanol	C4H6N2O	98	1.40
5	5.35	α-Pinene	C10H16	136	5.78
6	6.12	Cyclohexenone	C6H8O	96	1.14
7	6.50	Cinnamaldehyde	C9H8O	132	10.88
8	6.73	p-cymene	C10H14	134	2.87
9	6.92	4-Ketopimelic acid	C7H10O5	174	1.45
10	7.79	Alanine	C3H7NO2	89	1.13
11	8.21	Furanone	C4H4O2	84	0.02
12	8.75	Piperidine	C5H11N	85	0.56
13	9.17	Linalool	C10H18O	154	0.38
14	9.00	Linalyl isobutyrate	C14H24O2	224	0.11
15	9.84	Furaneol	C6H8O3	128	4.77
16	10.50	Thymine	C5H6N2O2	126	2.02
17	11.24	6-Hydroxy-5-decanone	C10H20O2	172	2.01
18	12.43	L-norvaline, n-ethoxycarbonyl-, butyl ester	C18H35NO4	245	2.87
19	12.70	L-valine, ethyl ester	C7H15NO2	145	0.77
20	13.78	4-Chloroanisole	ClC6H4OCH	143	1.31
21	13.98	Thiazole	C3H3NS	85	1.00
22	15.48	2,4-Difluoroaniline	C6H5F2N	129	2.62
23	15.87	Cyclopentanone, 2-(1-methylpropyl)-	C9H16O	140	0.81
24	16.05	5-hydroxymethylfurfural	C6H6O3	126	1.67
25	16.75	4-mercaptophenol	C6H6OS	126	1.36
26	17.69	D-allothreonine	C4H9NO3	119	1.44
27	19.10	Quinoline	C9H7N	129	5.29
28	20.58	Valproic acid	C8H16O2	144	0.57
29	20.97	2-ethylthiolane, s, s-dioxide	C6H12O2S	148	0.84
30	22.27	Eugenol	C10H12O2	164	10.19
31	26.69	Xanthosine	C10H12N4O6	284	9.10
32	27.32	Methylquinoline	C10H9N	143	4.97
33	29.07	Dodecanoic acid	C12H24O2	200	1.45

https://doi.org/10.2147/DDDT.S489113

According to the findings from DisGeNet web-server, the disease specificity index of matrix metalloproteinase-8 (MMP8) gene for diabetic wound disease was 0.488. The disease pleiotropy index for the gene MMP8 was 0.808. Gene-disease association score was 0.020 in case of MMP8. The results retrieved for matrix metalloproteinase-9 (MMP9) protein were 0.305 for diabetic wound disease specificity index, 0.923 for pleiotropy index and 0.090 for gene-disease association score.

Information from a wide range of sources, including public text collections, computer prediction techniques, and experimental data, is included in the STRING database. The first line of proteins which interact with MMP8 are TIMP1, TIMP4, TIMP2, A2M, ELANE, OLFM4, SERPINH1, MPO and DEFA4 (Figure 2a). The first line of protein–protein interactions for MMP9 occur with the following: THBS1, MMP1, TIMP1, TIMP2, LCN2, CTSG, TIMP3, ELN and DMP1 (Figure 2b).

The results collected for MMP8 from the ClinVar 2019 database showed that MMP8 and co-expressed genes have a p-value of 0.131 for diabetes mellitus disease. For the MMP9 protein, results showed that MMP9 and co-expressed genes have a p-value of 0.03448 for microvascular complications of diabetes. The adjusted p-value and odds ratio were 0.06113 and 33.49, respectively. The relationship between various diabetes-related pathologies and MMP8 is illustrated in a bar plot retrieved from Enrichr (Figure 3a and b). Similarly, the Diabetic Perturbations GEO 2022 database shows the connection between different diabetes-related pathologies and MMP9 in a bar plot (Figure 3c and d).

Evaluation of Binding Affinities of Ligands With Target Protein Through Molecular Docking

The potentials of the phytochemical ingredients to interact with MMP8 and MMP9 were investigated through the application of molecular docking. For MMP8 protein the top compounds with good binding affinities above −7 kcal/mol were xanthosine, methylquinoline, quinoline and L-norvaline, n-ethoxycarbonyl-, butyl ester respectively. The compound with the highest binding affinity toward MMP8 was xanthose with a binding affinity of −8.6 kcal/mol. For MMP9, the top compounds with binding affinities above −7 kcal/mol were quinoline and p-cymene (Table 2 and Figure 4).

Prediction of Absorption, Distribution, Metabolism and Excretion Profiles of Ligands

Inositol and 6-Hydroxy-5-decanone are P-glycoprotein substrates. All the ligands except furaneol, dodecanoic acid and 4-Ketopimelic acid showed a bioavailability score of 0.55. Furaneol and dodecanoic acid have bioavailability score of 0.85, while 4-Ketopimelic acid. Has a score of 0.56 Out of all the ligands, only 6-Hydroxy-5-decanone is CYP3A4 inhibitor. Eugenol, xanthosine, quinoline and methylquinoline are CYP1A2 inhibitors. The other ligands are not CYP1A2 inhibitors. Different parameters such as Molecular Weight, ESOL Class, GI absorption, BBB permeant and number of Lipinski violations have been tabulated from SwissADME (Table 3).

Biological Activity of Ligands

The structural formula is required to determine the expected biological activity profile for your compound; therefore, prediction can be performed even for virtual structures that have been computer-designed but not yet synthesized. The top 3 ligands with good binding affinities for each protein, MMP8 and MMP9 were subjected to investigation by PASS ONLINE. It is a sub-section of the way2drug web-server. The Pa score indicates probability of activity for each of the activity. The results retrieved from the web-server has been summarized in Table 4.

Molecular Dynamics Simulation Analysis

The Figure 5a and b and Figures S1 and S2 illustrate that the results of molecular dynamics simulations for protein-ligand complexes over 100 nanoseconds (ns). This plot shows the RMSD (root mean square deviation) values of the MMP8 protein with its docked Xanthosine compounds (ligand) (5a) and MMP9 protein with its docked Methylquinoline compounds (ligand) (5b) over time. The molecular dynamics simulations for protein-ligand complexes reveal that the MMP8 protein with Xanthosine and MMP9 protein with Methylquinoline exhibit gradual increases in RMSD values over 100 ns, stabilizing around 2.5 nm and 7.5 nm, respectively, indicating conformational changes while maintaining relative

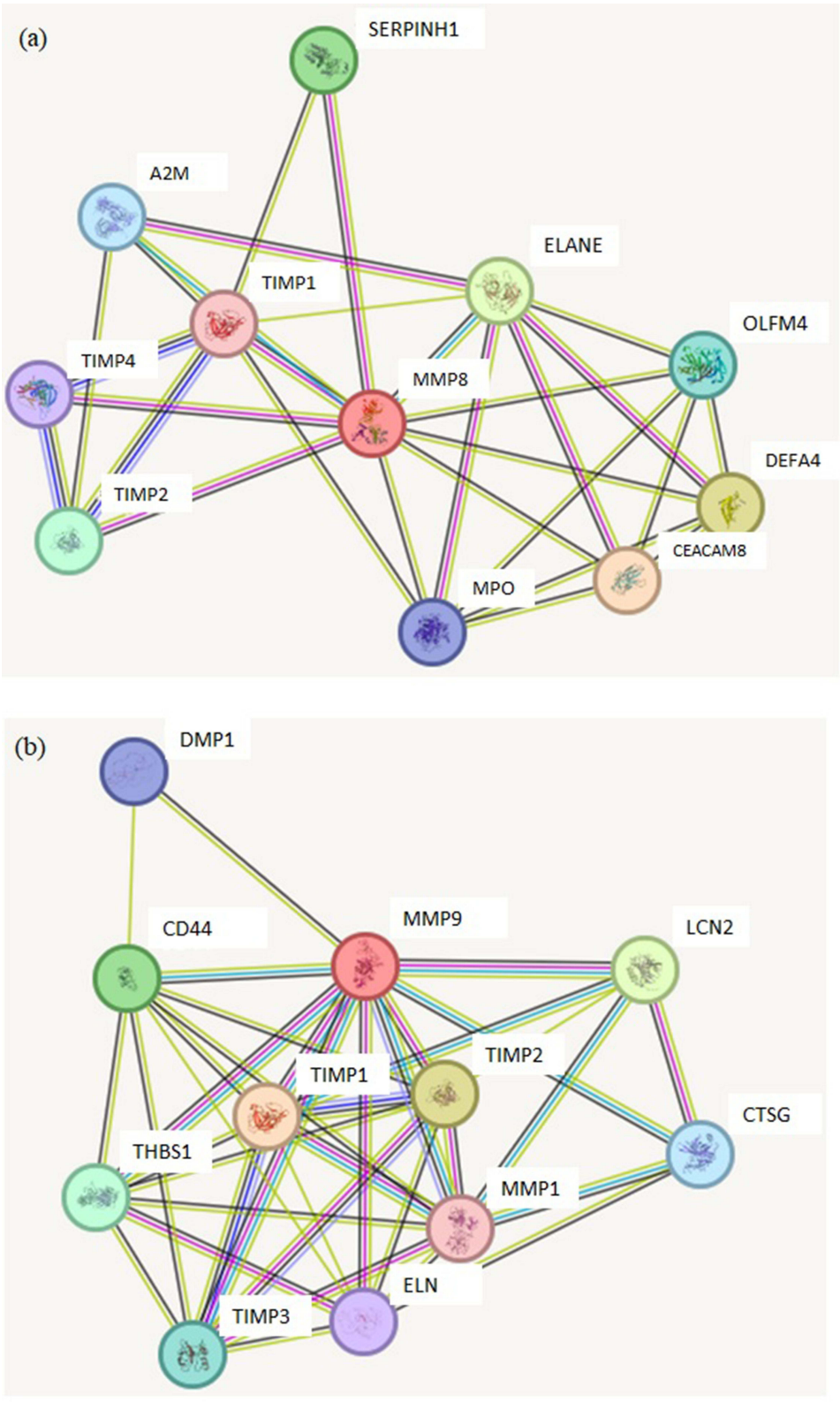

Figure 2 Protein-protein network of (**a**) MMP8 and (**b**) MMP9 proteins generated using STRING platform.

https://doi.org/10.2147/DDDT.S489113

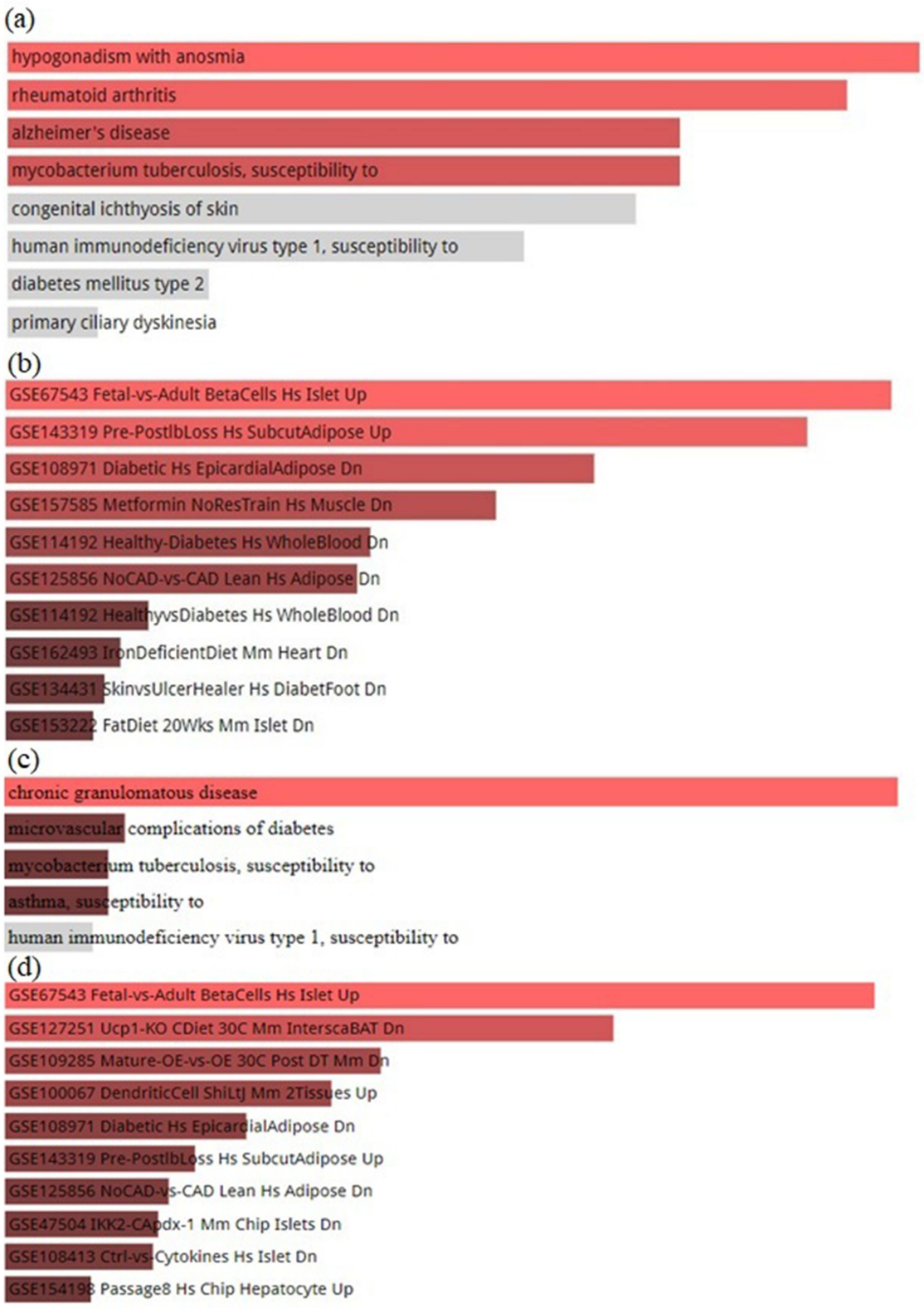

Figure 3 Bar plot retrieved from (**a**) ClinVar 2019 and (**b**) Diabetic perturbation GEO 2022 archives through Enrichr for MMP8 protein and (**c**) ClinVar 2019 and (**d**) Diabetic perturbation GEO 2022 archives through Enrichr for MMP9 protein. The bar plots are sorted based on p-value ranking.

Table 2 Binding Affinities of Phytochemicals Docked With MMP8 and MMP9 Proteins

Ligands	Binding Affinity with MMP8 (kcal/mol)	Binding Affinity with MMP9 (kcal/mol)
Xanthosine	−8.6	−7.2
Methylquinoline	−7.8	−7.9
Quinoline	−7.3	−7.6
L-norvaline, n-ethoxycarbonyl-, butyl ester	−7.3	−6.6
p-cymene	−6.8	−7.0
4-Ketopimelic acid	−6.6	−6.5
Eugenol	−6.5	−5.3
Linalyl isobutyrate	−6.4	−5.3
Cinnamaldehyde	−6.4	−6.6
Thymine	−6.2	−6.4
Dodecanoic acid	−6.2	−4.5
2,4-Difluoroaniline	−6.2	−5.8
Cyclopentanone, 2-(1-methylpropyl)-	−6.2	−5.6
Valproic acid	−6	−6.1
Linalool	−6	−4.8
Furaneol	−6	−4.9
α-Pinene	−5.9	−5.5
Inositol	−5.8	−6.7
5-hydroxymethylfurfural	−5.8	−6.1
6-Hydroxy-5-decanone	−5.7	−6.3
4-Chloroanisole	−5.6	−5.9
4-mercaptophenol	−5.3	−5.6
L-valine, ethyl ester	−5.2	−5.6
Cyclohexenone	−5.1	−5.1
D-allothreonine	−4.8	−5.2
2-ethylthiolane, s, s-dioxide	−4.7	−4.6
Imidazole-4-methanol	−4.6	−5.1
Furanone	−4.5	−4.7
Alanine	−4.4	−4.6
Piperidine	−4.3	−4.9
Glycine	−3.7	−3.9
Thiazole	−3.4	−3.9
Cyclobutanethiol	−3.4	−4.0

https://doi.org/10.2147/DDDT.S489113

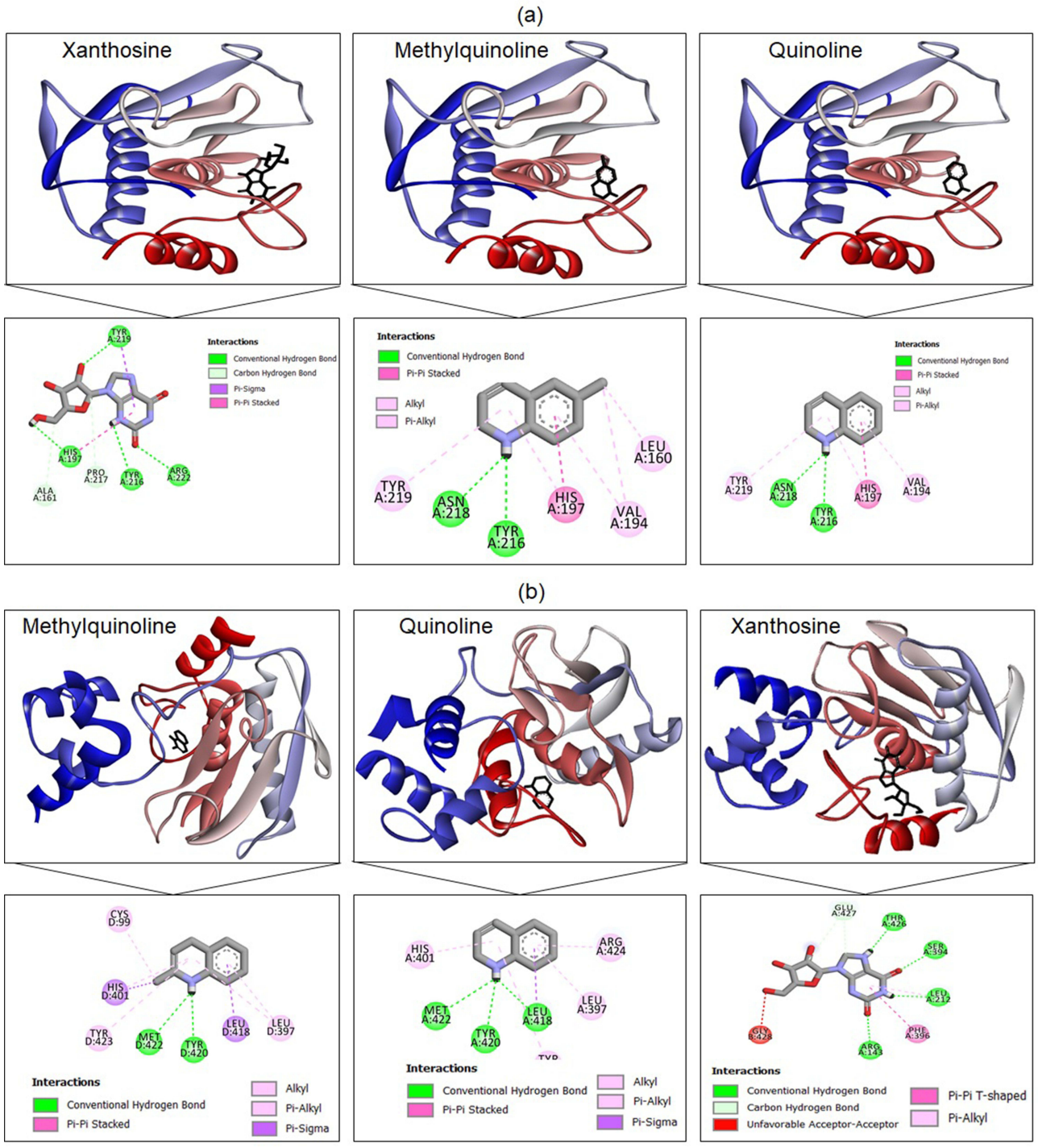

Figure 4 Protein-ligand docked complexes of compounds with good binding towards target proteins MMP8 (**a**) and MMP9 (**b**) for top three ligands along with 2D interaction diagrams.

stability. In contrast, the ligands show lower RMSD values, fluctuating between 1.0 to 1.5 nm for MMP8 and 1.5 to 4.0 nm for MMP9, demonstrating that they remain stable and well-aligned with the proteins during the simulations (Table 5). The RMSD plots show that both MMP8 and MMP9 proteins, along with their respective ligands, maintain stability throughout the 100 ns simulation. The protein conformational changes are within the acceptable range, indicating that the protein-ligand complexes are stable.

Table 3 ADME Parameters of 33 Ligands Tabulated From SwissADME Web-Server

Ligand	MW	ESOL Class	GIT Absorption	BBB permeant	Lipinski #violations
Xanthosine	284.23	Very soluble	Low	No	0
Methylquinoline	143.19	Soluble	High	Yes	0
Quinoline	129.16	Soluble	High	Yes	0
L-norvaline, n-ethoxycarbonyl-, butyl ester	307.38	Soluble	High	Yes	0
p-cymene	134.22	Soluble	Low	Yes	1
4-Ketopimelic acid	174.15	Highly soluble	High	No	0
Eugenol	164.2	Soluble	High	Yes	0
Linalyl isobutyrate	224.34	Soluble	High	Yes	0
Cinnamaldehyde	132.16	Soluble	High	Yes	0
Thymine	126.11	Very soluble	High	No	0
Dodecanoic acid	200.32	Soluble	High	Yes	0
2,4-Difluoroaniline	129.11	Soluble	High	Yes	0
Cyclopentanone, 2-(1-methylpropyl)-	140.22	Soluble	High	Yes	0
Valproic acid	144.21	Soluble	High	Yes	0
Linalool	154.25	Soluble	High	Yes	0
Furaneol	128.13	Very soluble	High	Yes	0
α-Pinene	136.23	Soluble	Low	Yes	1
Inositol	180.16	Highly soluble	Low	No	1
5-hydroxymethylfurfural	126.11	Very soluble	High	No	0
6-Hydroxy-5-decanone	354.36	Moderately soluble	High	No	0
4-Chloroanisole	142.58	Soluble	High	Yes	0
4-mercaptophenol	126.18	Very soluble	High	Yes	0
L-valine, ethyl ester	145.2	Very soluble	High	Yes	0
Cyclohexenone	96.13	Very soluble	High	Yes	0
D-allothreonine	119.12	Highly soluble	High	No	0
2-ethylthiolane, s, s-dioxide	148.22	Very soluble	High	Yes	0
Imidazole-4-methanol	98.1	Very soluble	High	No	0
Furanone	84.07	Very soluble	High	No	0
Alanine	89.09	Highly soluble	High	No	0
Piperidine	85.15	Very soluble	Low	No	0
Glycine	75.07	Highly soluble	High	No	0
Thiazole	85.13	Very soluble	High	Yes	0
Cyclobutanethiol	88.17	Very soluble	High	Yes	0

Table 4 Probability of Activity (Pa) Scores for the Various Biological Activities of Top Ligands With Good Binding Affinities Towards Target Proteins

Ligands	Biological Activities	Pa Value
Xanthosine	Isopenicillin-N epimerase inhibitor	0.810
	Antiviral (Picornavirus)	0.804
	Antiviral (Poxvirus)	0.931
	Immunostimulant	0.832
Methylquinoline	Cytochrome P450 stimulant	0.836
	Thioredoxin inhibitor	0.802
	Testosterone 17beta-dehydrogenase (NADP+) inhibitor	0.811
Quinoline	Glycosylphosphatidylinositol phospholipase D inhibitor	0.954
	Dehydro-L-gulonate decarboxylase inhibitor	0.940
	Carboxypeptidase Taq inhibitor	0.937
	Phthalate 4.5-dioxygenase inhibitor	0.929
	Glutathione thiolesterase inhibitor	0.929
	Pullulanase inhibitor	0.929
	Aldehyde dehydrogenase (pyrroloquinoline-quinone) inhibitor	0.925
	Nitrate reductase (cytochrome) inhibitor	0.925
	Amine dehydrogenase inhibitor	0.921
	(R)-6-hydroxynicotine oxidase inhibitor	0.920

In the Figure 5c and d, This plot presents the RMSF (root mean square fluctuation) values for the C-alpha atoms of the MMP8 and MMP9 proteins over the residue index. Peaks in RMSF values indicate regions of higher flexibility within the MMP8 protein. Residues with RMSF values of MM8 were up to 4.0 Å exhibit considerable motion, possibly corresponding to loops or unstructured regions. Similar to MMP8, peaks in RMSF values indicate regions of higher flexibility in the MMP9 protein. The fluctuations range up to 9.0 Å, suggesting some residues or regions are highly flexible. The RMSF plots reveal specific regions of flexibility within the proteins. Identifying these regions can be crucial for understanding the dynamics and potential binding sites of the proteins.

Figure 6a and d illustrates that the interaction diagrams of molecular dynamics (MD) simulations for target protein-drug complexes. Specifically, it shows the interactions of MMP8 complexed with Xanthosine and MMP9 complexed with Methylquinoline. This diagram (6a-b) shows the chemical structure of Xanthosine molecule includes multiple functional groups such as hydroxyl (OH) groups and amine (NH2) groups. It likely forms hydrogen bonds and other interactions with the target protein (MMP8) during the MD simulation. Residues such as HIS, LEU, ASN, PRO, and GLU are involved in interactions with Xanthosine, indicating hydrogen bonds, electrostatic interactions, and possibly hydrophobic contacts. Xanthosine interacts with several residues in MMP8, forming a network of interactions that stabilize the complex. The interaction is facilitated by hydrogen bonds and possibly hydrophobic contacts. This diagram (6c-d) shows the chemical structure of Methylquinoline consists of a quinoline ring structure with a methyl group substitution and nitrogen in the ring may participate in interactions with the protein (MMP9). TYR 420 is identified as a significant interacting residue, with a 99% interaction rate, indicating a strong and consistent interaction with Methylquinoline during the simulation. Methylquinoline primarily interacts with TYR 420 in MMP9, forming a strong

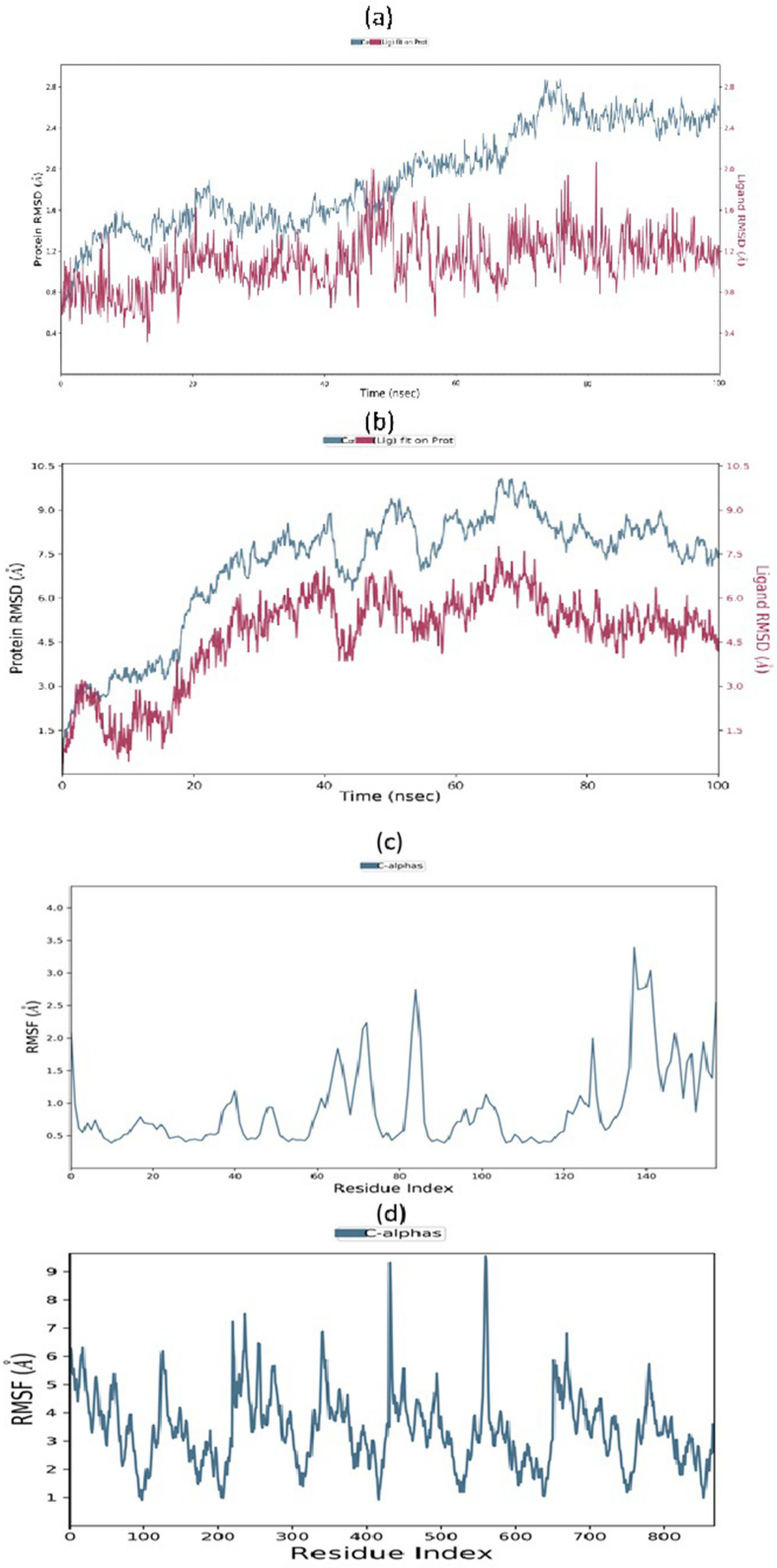

Figure 5 Trajectory plots of molecular dynamics (MD) of target protein-drug complex. Protein ligand-root mean square deviation (PL-RMSD) with respect to time (nanoseconds) during MD simulation of MMP8 complexed with xanthosine (**a**) and MMP9 complexed with methylquinoline (**b**). Protein-root mean square fluctuation (P-RMSF) with respect to time (nanoseconds) during MD simulation of MMP8 complexed with xanthosine (**c**) and MMP9 complexed with methylquinoline (**d**).

https://doi.org/10.2147/DDDT.S489113

Table 5 Average, Maximum and Minimum Protein-RMSD and Ligand-RMSD With Respect to Time (Nanoseconds) During MD Simulation of MMP8 Complexed With Xanthosine and MMP9 Complexed With Methylquinoline

MD Simulation Trajectories	Xanthosine			Methylquinoline		
	Average	Maximum	Minimum	Average	Maximum	Minimum
Protein RMSD	2.0 Å	2.8 Å	0.6 Å	7.50 Å	9.6 Å	1.0 Å
Ligand bound RMSD	1.20 Å	2.0 Å	0.3 Å	4.50 Å	7.50 Å	1.0 Å

Abbreviations: RMSD, ligand-root mean square deviation; RMSF, root mean square fluctuation.

and consistent interaction. This suggests a significant role for TYR 420 in stabilizing the Methylquinoline-MMP9 complex.

Figure 7 presents normalized stacked interaction bar charts derived from molecular dynamics simulations focusing on two distinct protein-drug complexes. It illustrates the interactions between the MMP8 protein interected with xanthosine and MMP9 protein with methylquinoline, employing color-coded bars to represent various interaction types, including hydrogen bonds, hydrophobic interactions, and water bridges, thereby facilitating an intuitive comparison of their relative

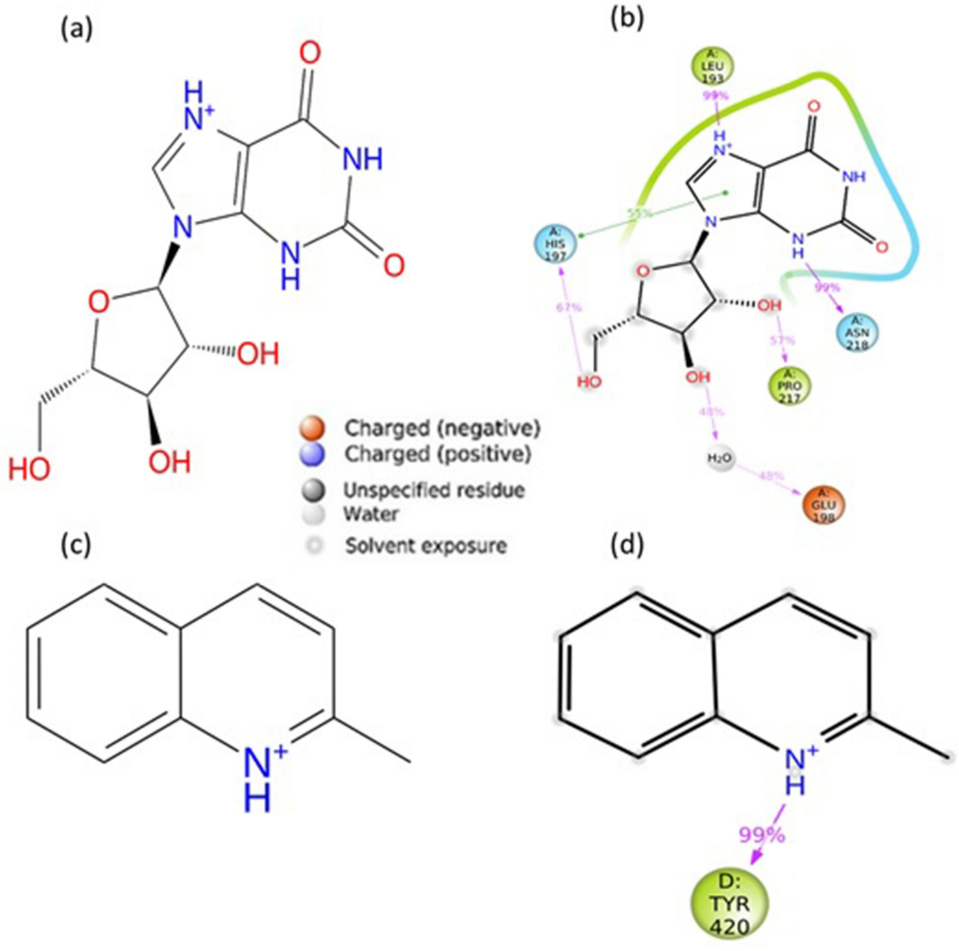

Figure 6 Trajectory plots of molecular dynamics (MD) of target protein-drug complex. Interaction plots of molecular dynamics (MD) of target protein-drug complex. Interaction diagram during MD simulation of MMP8 complexed with xanthosine (**a** and **b**) and MMP9 complexed with methylquinoline (**c** and **d**). Color labels at the center signify the interaction taking place for the circles.

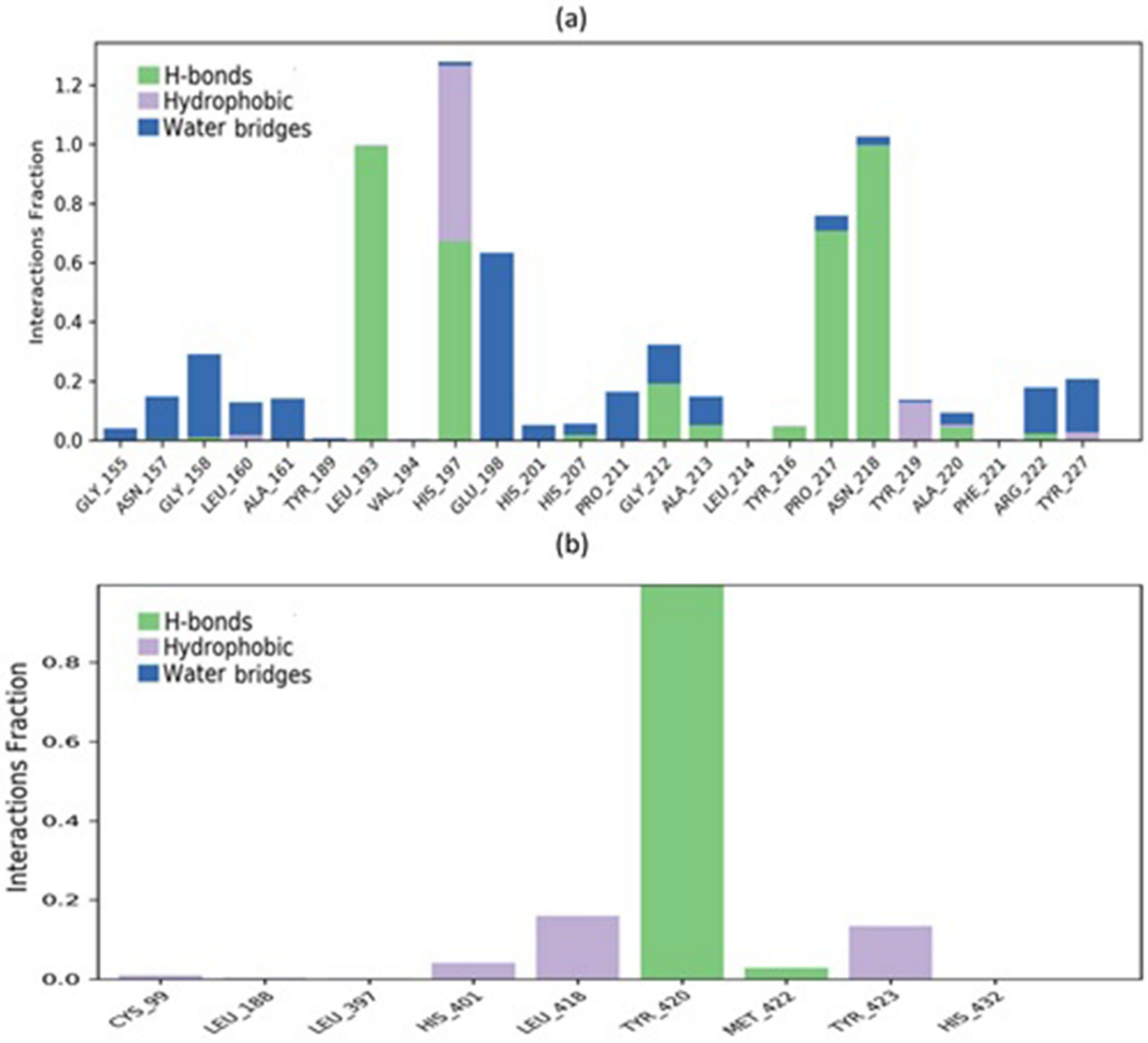

Figure 7 Normalized stacked interaction bar charts during MD simulation of MMP8 complexed with xanthosine (**a**) and MMP9 complexed with methylquinoline (**b**). Color labels signify the interaction taking place for each column.

significance. These charts effectively highlight the differences in interaction patterns among various amino acids within each protein throughout the course of the simulation.

Assessment of In-Vivo Diabetic Wound Healing

Macroscopic Assessment and Wound Contraction Measurement

Macrocosmic view in the Figure 8 showed that the wound healing efficacy of a CZ extract treatment against standard povidone-iodine and a vehicle control in diabetic and non-diabetic mice revealed that CZ extract significantly accelerated wound healing. Wounds treated with CZ extract began healing around day 10, compared to day 14 for both the negative control group and vehicle control groups. This accelerated healing was attributed to a faster transition through the wound healing stages, with CZ extract-treated wounds displaying signs of moving from the inflammatory to the proliferation stage by day 3. Additionally, CZ extract facilitated rapid scab formation and granulation tissue development, leading to earlier appearance of white fibrous tissue. The non-diabetic group exhibited the fastest healing, while the standard

https://doi.org/10.2147/DDDT.S489113

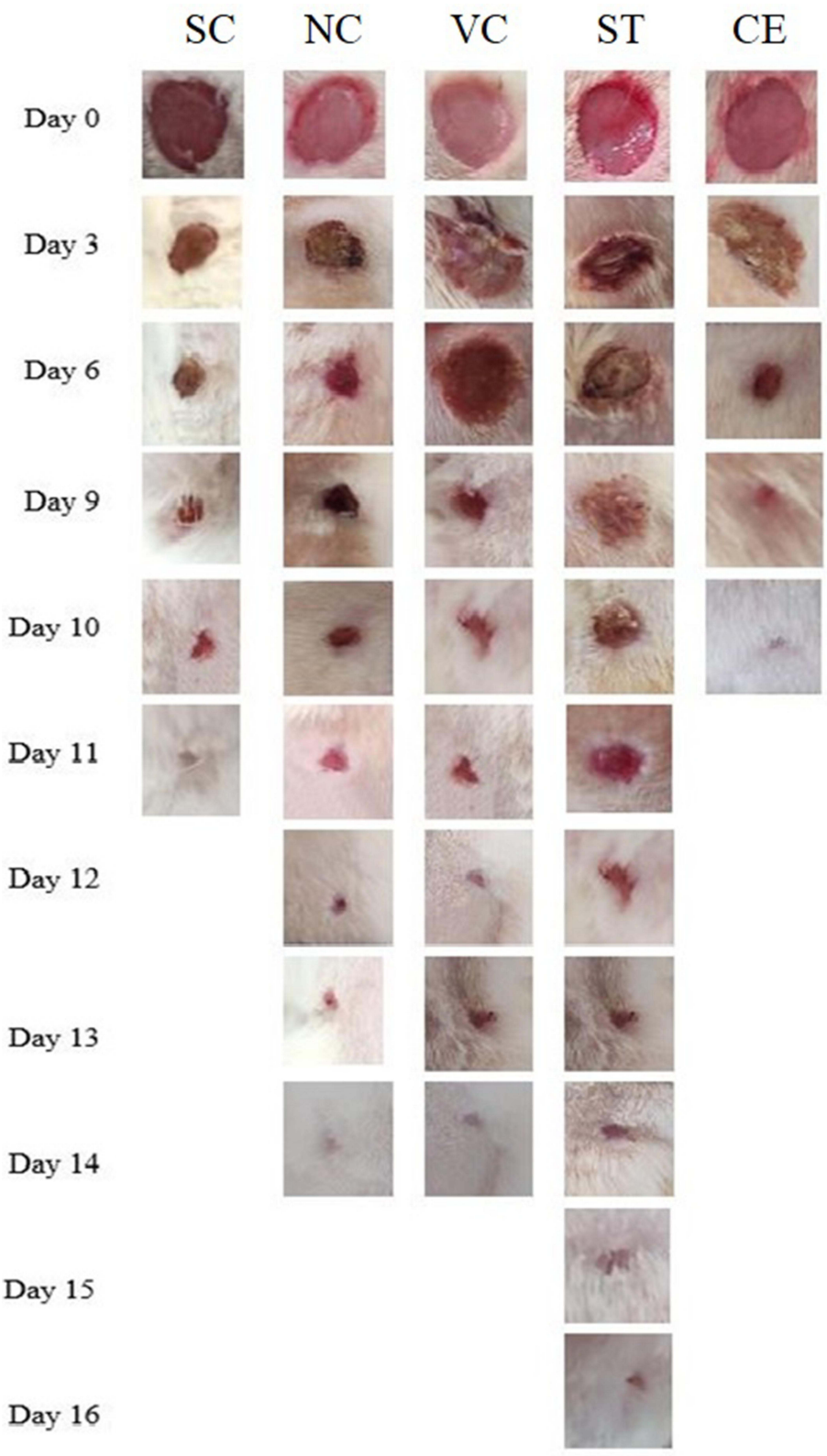

Figure 8 Macroscopic view of wounds of five experimental groups: SC, NC, VC, ST and CE on day 0, 3, 6, 9, 10, 11, 12, 13, 14, 15 and 16. SC, non-diabetic sham control, NC, diabetic negative control (without treatment), VC, diabetic vehicle control, ST, treated with povidone-iodine as standard treatment, and CE, treated group with CZ extract.

Table 6 Wound Surface Area of Five Experimental Groups: SC, NC, VC, ST and CE

Groups	Wound Surface Area (mm)					
	Day 0	Day 3	Day 6	Day 9	Day 10	Day 11
SC	69.87 ± 3.91	39.94 ± 2.17	29.68 ± 2.63	12.32 ± 1.48	6.96 ± 1.48	4.48 ± 1.11
NC	57.18 ± 4.11	62.93 ± 3.23	40.24 ± 3.59	22.99 ± 4.36	14.16 ± 2.34	9.46 ± 1.94
VC	67.95 ± 3.69	64.13 ± 3.00	45.57 ± 3.68	22.83 ± 2.23	18.51 ± 2.50	12.96 ± 2.06
ST	69.24 ± 6.25	71.14 ± 5.81	51.35 ± 3.35	30.93 ± 3.12	22.45 ± 2.96	17.55 ± 2.95
CE	67.25 ± 3.90	45.13 ± 3.29*	19.07 ± 1.95**	2.71 ± 0.97**	0.81 ± 0.40**	0.00 ± 0.00**

Notes: All data are given as mean ± S.E. for six animals in each group. Statistically significant results are indicated as *$p < 0.05$, CE versus NC, VC and ST and **$p < 0.000$, CE versus SC, NC, VC and ST.

treatment group required approximately 16 days for full recovery. These findings highlight the potential of CZ extract as a promising therapeutic agent for accelerating wound healing in diabetic individuals.

Wound surface area on day basis is described in the Table 6 and S2. At day zero, there were no significant differences among the groups, ensuring a fair comparison. By day 3, the CZ extract-treated group (CE) showed a statistically significant reduction in wound area (45.13 ± 3.29 mm) compared to the NC, VC, and ST groups, although no significant difference was found between the CE and SC groups. CE group demonstrated faster healing on Day 6, 9, and 10, with significantly lower wound areas ($p < 0.001$) compared to all other groups, including SC, NC, VC, and ST. These results suggest that CZ extract has notable wound healing properties, especially for diabetic wounds.

The complete healed of wounds data are presented in Figure 9 offers valuable insights into the effectiveness of experimental treatments. The results showed that CE group treated with CZ extract, experienced a significantly faster healing process compared to the untreated and control groups (SC, NC, VC, and ST). Statistical analysis revealed that the difference in the mean day of complete wound healing for the CE group was statistically highly significant ($p < 0.000$). Notably, the NC group, representing the diabetic negative control, exhibited the slowest healing time, highlighting the detrimental effect of diabetes on wound recovery. In addition, the SC group, comprising non-diabetic mice, demonstrated relatively quick healing, faster than the NC group. There was no significant difference in healing times between the VC

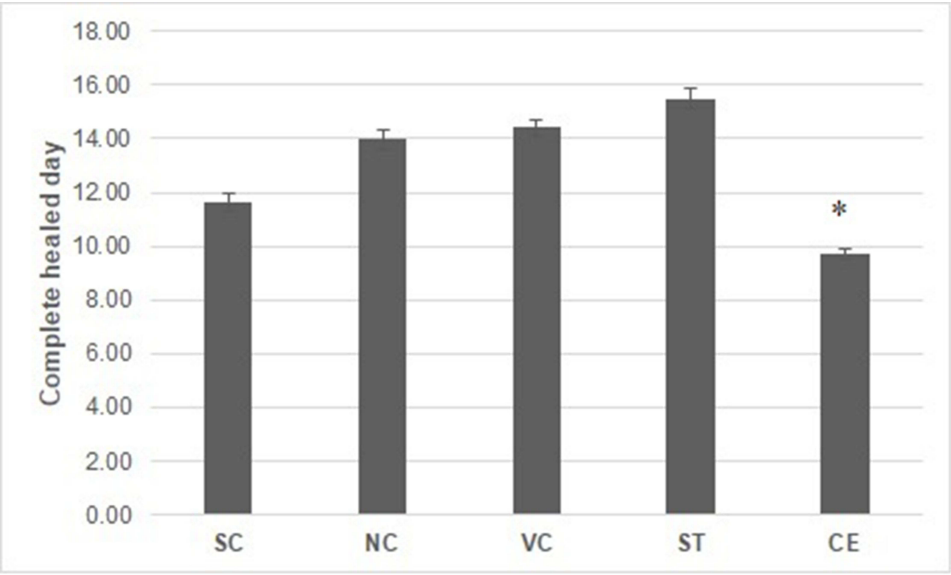

Figure 9 Bar charts represent of complete healed day of five experimental groups: SC, NC, VC, ST and CE. All data are given as mean ± S.E. for six animals in each group. Statistically significant results are indicated as *$p < 0.000$, CE versus SC, NC, VC and ST.

https://doi.org/10.2147/DDDT.S489113

and NC groups. Both groups (NC and VC) taken duration for completing healed around 14 days. Moreover, povidone-iodine treatment group (ST) demonstrated a relatively slower wound healing rate, as shown by the similar outcomes within these conditions. ST took to complete cover the wounds more than 16 days. These findings highlight the potential therapeutic benefits of CZ extract in promoting faster wound healing, which could have important clinical applications.

Determination of Hydroxyproline Content

Figure 10 shows the content of hydroxyproline in skin tissue on post-wounded day 3 and day 9 of five experimental groups: SC, NC, VC, ST and CE. At the early stage of wound treatment (Day 3), the hydroxyproline content ranged from 41.02 ± 0.37 to 47.49 ± 025 mg/g, and there was no significant difference among the groups. On day 9, the hydroxyproline content in CZ treated group (60.82 ± 0.62 mg/g) was significantly higher ($p < 0.001$) than the NC (45.12 ± 0.95 mg/g), VC (54.31 ± 1.50 mg/g), and ST (47.03 ± 0.91 mg/g) groups. A similar trend had been shown in the non-diabetic sham control (SC) group. Hydroxyproline content of SC group was 57.84 ± 0.54 mg/g ($p < 0.0001$, versus NC and ST). Notably, hydroxyproline content increased gradually after day 3 for the most of groups such as SC, NC, VC and CE. However, ST group remained steady results between day 3 (47.49 ± 0.25 mg/g) and day 9 (47.03 ± 0.91 mg/g). In addition, there was no significant difference between NC and ST groups ($p = 0.636$).

Antioxidant Enzyme Activities

Figure 11a shows the level of catalase (Cat) in skin tissue on post-wounded day 3 and day 9 of five experimental groups: SC, NC, VC, ST and CE. At the early stage of wound treatment (Day 3), the Cat levels ranged from 71.36 ± 6.00 to 98.90 ± 4.57 U/g, and there was no significant difference among the groups. On day 9, the Cat levels in SC (179.01 ± 15.99 U/g) ($p < 0.05$), VC (172.89 ± 21.87 U/g) ($p < 0.05$) and CE (220.49 ± 18.35 U/g) ($p < 0.0001$) groups was significantly higher compared to NC group (99.78 ± 9.44 U/g). An opposite trend had been shown in the standard treatment (ST) group. There was no significant difference between NC and ST groups ($p = 0.136$).

Figure 11b shows the level of reduced glutathione (GSH) in skin tissue on post-wounded day 3 and day 9 of five experimental groups: SC, NC, VC, ST and CE. At day 3, GSH levels ranged were from 247.69 ± 1.87 to 321.75 ± 25.01 μg/g among the groups. They had no significant difference. Later stage on day 9, the GSH levels in SC (743.52 ± 49.69 μg/g) ($p < 0.0001$), VC (638.26 ± 20.88 μg/g) ($p < 0.01$) and CE (736.12 ± 62.12 μg/g) ($p < 0.0001$) groups was significantly higher compared to NC group (419.89 ± 39.43 μg/g). However, ST group showed remained steady results like NC group on the corresponding day and no significant difference between them ($p = 0.772$).

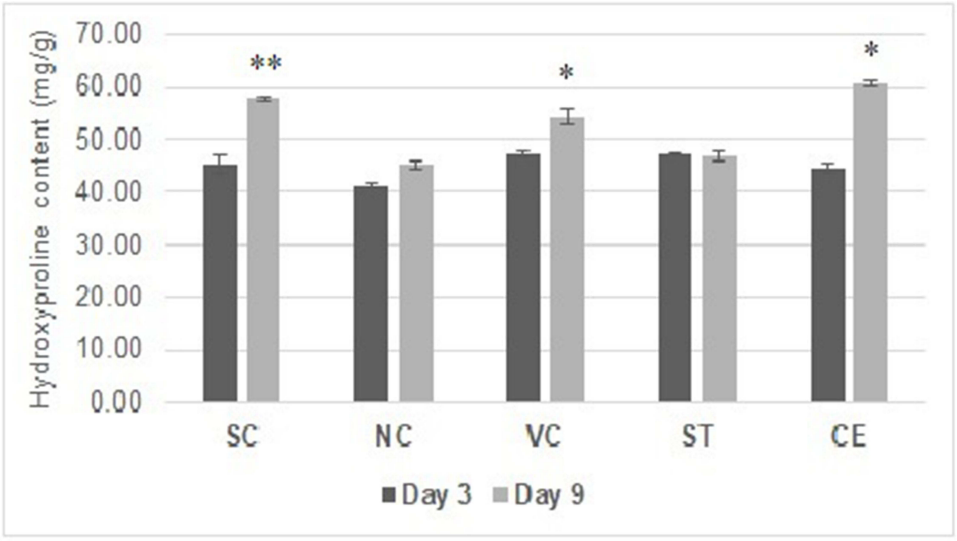

Figure 10 Bar charts represent of hydroxyproline content (mg/g) of skin tissue on post-wounded day 3 (Bold) and day 9 (light) of five experimental groups: SC, NC, VC, ST and CE. All data are given as mean ± S.E. for six animals in each group. Statistically significant results are indicated as *$p < 0.001$, CE versus NC, VC and ST; VC versus NC; **$p < 0.0001$, SC versus NC and ST; and $p = 0.636$, ST versus NC on the corresponding day.

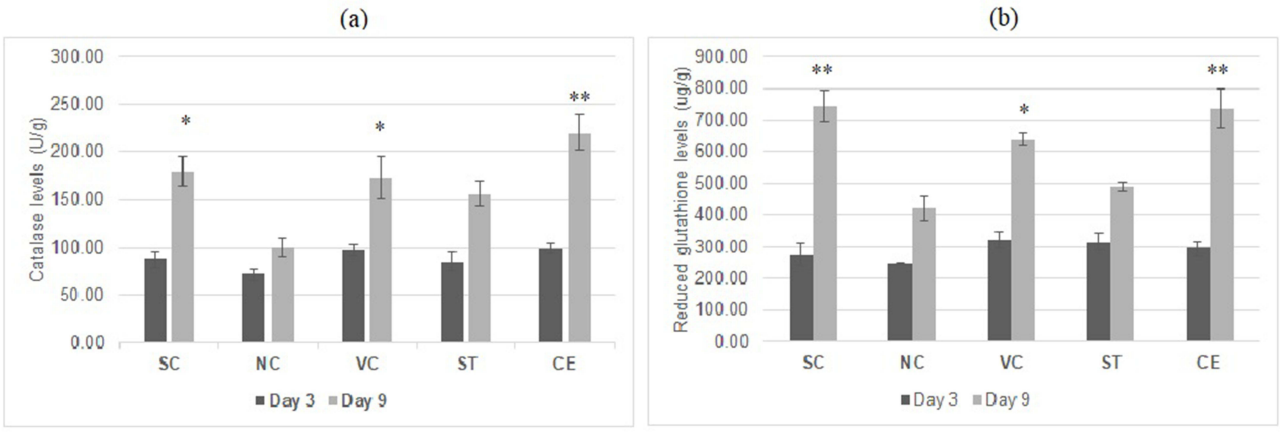

Figure 11 Bar charts represent of catalase (Cat) levels (U/g) (**a**) and reduced glutathione (GSH) levels (ug/g) (**b**) of skin tissue on post-wounded day 3 (Bold) and day 9 (light) of five experimental groups: SC, NC, VC, ST and CE. All data are given as mean ± S.E. for six animals in each group. In case of (**a**), statistically significant results are indicated as $*p < 0.05$, SC and VC versus NC; $**p < 0.0001$, CE versus NC; $p = 0.136$, ST versus NC on the corresponding day and in case of (**b**), statistically significant results are indicated as $*p < 0.01$, VC versus NC; $**p < 0.0001$, CE and SC versus NC; $p = 0.772$, ST versus NC on the corresponding day.

Estimation of Lipid Peroxidation

Figure 12 shows the levels of Malondialdehyde (MDA) in skin tissue on post-wounded day 3 and day 9 of five experimental groups: SC, NC, VC, ST and CE. There was no significant difference from day 3 to day 9 among groups except CE. MDA levels reduced in SC, NC and CE groups and increased in VC and ST groups from day 3 to day 9. However, only MDA levels of CE group at day 9 (32.91 ± 0.51 nmol/g) was significantly lower ($p < 0.01$) that day 3 (46.06 ± 0.67 nmol/g). In addition, MDA levels in CE group (32.91 ± 0.51 nmol/g) was significantly lower ($p < 0.05$) compared to VC (39.87 ± 1.89 nmol/g) and ST (41.85 ± 3.83 nmol/g) groups on the corresponding day 9.

Assessment of Skin Tissue Histomorphology

Histopathological examination of the wound tissues was carried out using hematoxylin and eosin (H&E) for evaluation of skin morphology. In the Table 7, histological observations of re-epithelialization, fibroblast cell proliferation,

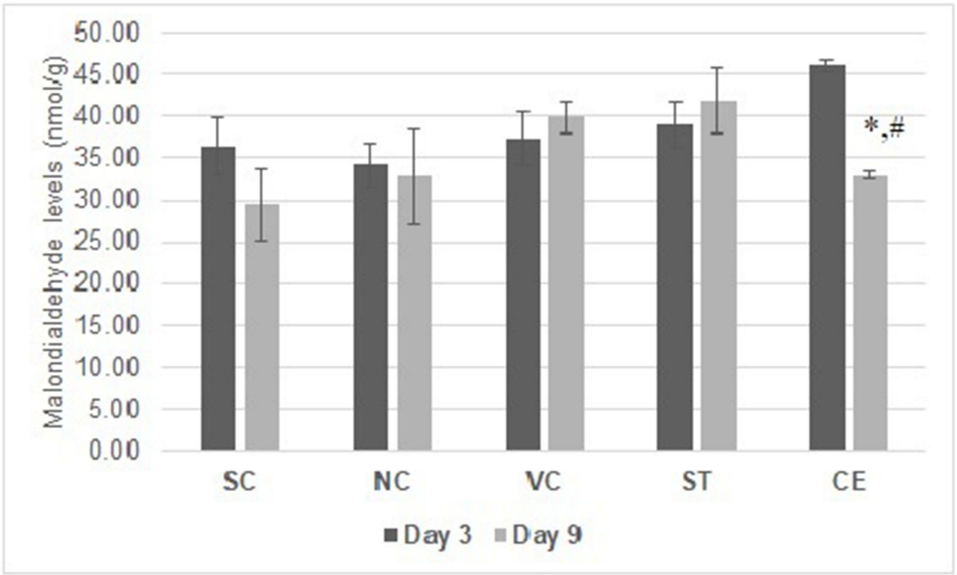

Figure 12 Bar charts represent of malondialdehyde (MDA) levels (nmol/g) of skin tissue on post-wounded day 3 (Bold) and day 9 (light) of five experimental groups: SC, NC, VC, ST and CE. All data are given as mean ± S.E. for six animals in each group. Statistically significant results are indicated as $*p < 0.05$, CE and SC versus ST on the corresponding day and $^{\#}p < 0.001$, Day 3 versus Day 9 of CE group.

https://doi.org/10.2147/DDDT.S489113

Table 7 Mean Score From Histological Evaluation of Skin Tissue on Post-Wounded Day 3 and Day 9 by Hematoxylin and Eosin (H&E) Staining of Five Experimental Groups: SC, NC, VC, ST and CE

Groups	Re-Epithelialization		Inflammatory cell Infiltration		Fibroblast cell Proliferation		Neo-Vascularization		Granulation Tissue Formation	
	Day 3	Day 9	Day 3	Day 9	Day 3	Day 9	Day 3	Day 9	Day 3	Day 9
SC	0.00 ± 0.00	1.67 ± 0.17	2.06 ± 0.10	1.06 ± 0.06	0.94 ± 0.06	1.72 ± 0.09	0.50 ± 0.12	1.83 ± 0.08	0.78 ± 0.15	1.94 ± 0.06
NC	0.00 ± 0.00	1.22 ± 0.32	1.89 ± 0.07	1.50 ± 0.12	0.89 ± 0.07	1.67 ± 0.08	0.56 ± 0.10	1.89 ± 0.07	0.78 ± 0.12	1.89 ± 0.07
VC	0.00 ± 0.00	1.67 ± 0.17	1.89 ± 0.07	1.17 ± 0.08	0.83 ± 0.08	1.83 ± 0.08	0.83 ± 0.12	1.94 ± 0.06	0.67 ± 0.08	1.61 ± 0.16
ST	0.33 ± 0.17	2.00 ± 0.00	1.94 ± 0.06	1.17 ± 0.08	0.78 ± 0.12	1.89 ± 0.11	0.72 ± 0.12	1.94 ± 0.06	0.44 ± 0.15	1.94 ± 0.06
CE	0.33 ± 0.17	2.94 ± 0.06[a]	2.39 ± 0.07[b]	0.67 ± 0.14[c]	1.00 ± 0.00	2.61 ± 0.11[d]	1.11 ± 0.07[e]	2.06 ± 0.06	1.11 ± 0.07	2.83 ± 0.08[f]

Notes: All data are given as mean ± S.E. for six animals in each group. Statistically significant results are indicated as [a]$p < 0.0001$, CE versus SC, NC and VC and $p < 0.01$, CE versus ST on the corresponding day; [b]$p < 0.0001$, CE versus NC and VC; $p < 0.01$, CE versus ST and $p < 0.05$, CE versus SC on the corresponding day; [c]$p < 0.0001$, CE versus NC and $p < 0.05$, CE versus VC and ST on the corresponding day; [d]$p < 0.0001$, CE versus SC, NC, VC and ST on the corresponding day; [e]$p < 0.01$, CE versus SC and NC on the corresponding day; and [f]$p < 0.0001$, CE versus SC, NC, VC and ST on the corresponding day.

neovasculation, and granulation tissue development were all identical in all groups; however, inflammatory cell infiltration was diametrically opposed. On day 3, skin histology as evaluated by H&E stain were immature in all characteristics except for inflammatory cell infiltration, where the score varied from around 0 to 1. When the healing process had progressed further, the cells were abundant and completely matured. However, the score for inflammatory cell infiltration was the complete reverse. On day 3, the inflammatory cells scored between 1.9 and 2.4, suggesting a mild to severe infiltration. Moreover, at the early stage (day 3), parameters of histology such as proliferation of epithelial cells, vascular cells, and granulation tissues in wounded skin were immature and the score was around 1. By day 9, most of the parameters were matured in the treated groups with a score of 2 to 3, whereas the control groups were less matured than treated groups on the corresponding days. The mean scores from histological evaluations on days 3 and 9 demonstrated statistically significant differences, particularly for the CE group, which consistently showed higher scores compared to SC, NC, VC, and ST groups, with p-values indicating strong significance ($p < 0.0001$). This data underscores the effectiveness of the treatments in promoting wound healing.

Figure 13 shows the histomorphological view of the wounded skin by H&E staining of the SC, NC, VC, ST and CE groups on days 3 and 9 post-wounding. The pictures of skin histology illustrated that on day 3, there were many inflammatory cells on necrotic cells layer. The skin microstructure at the wound site such as epidermal, dermal, and hypodermal was not prominent at an early stage, as indicated by the lacking proliferation of epithelial cell, fibroblast, and granulation tissue formation. However, on day 9, inflammatory cells still appeared in the wounding area and the epidermal layer was not mature enough in the control groups whereas these were improved significantly in the treated groups. The wound healing process in the treated groups was recovered by epithelialization with the formation of keratinocytes at the same time. Newly formed capillary, fibroblast, collagen, and connective tissues were seen in the treated groups on day 9, whereas the formation of fibroblast cells, granulation tissue, and, eventually, the re-epithelialization of wound skin in the control groups were delayed and formed on days 11 to 16. Overall, the skin structure was more matured in the treated groups compared to the control groups at the later stage.

CZ Effects on Diabetic Condition and

To optimize the diabetic condition of the experimental groups, various glucose parameters such as fasting blood glucose (FBG) levels, and oral glucose tolerance test (OGTT) had been done before starting treatment. In addition, serum glucose level was measured to make sure the steady diabetic condition throughout the experiment. In the Table 8 shows that before alloxan induction, FBG levels was almost similar results in all experimental groups and there was no significant difference among them. However, after alloxan induction, FBG level of diabetic groups (NC, VC, ST and CE) was significantly increased ($p < 0.0001$) than non-diabetic group (SC). A similar result had been shown in the OGTT test. After alloxan induction, OGTT was remained significant difference ($p < 0.0001$) between diabetic () and non-diabetic

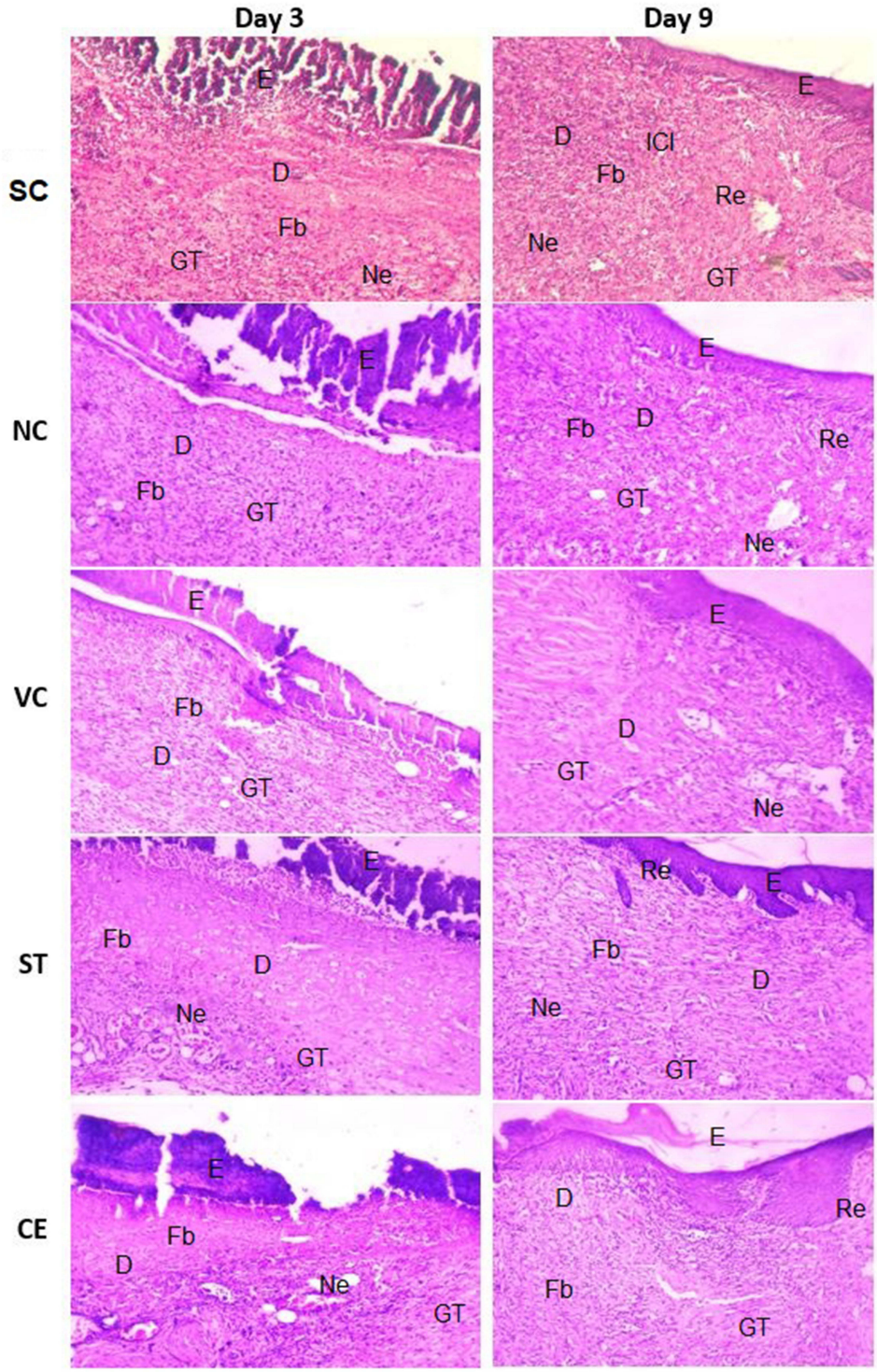

Figure 13 Histopathological view of skin tissue on post-wounded day 3 and day 9 by hematoxylin and eosin (H&E) staining of five experimental groups: SC, NC, VC, ST and CE. Pictures of stain are at 10x magnification. Bar scale: 100 µm.
Abbreviations: E, Epidermis; D, Dermis; Fb, Fibroblast cells; ICl, Inflammatory cells infiltration; Re, Re-epithelialization; Ne, Neo-vascularization; GT, Granulation tissue.

groups at both 0 (zero) min and 120 min. A dramatic change was seen during treatment in case of serum glucose level. The level of serum glucose of SC group at day 3 (5.53 ± 0.33) and day 9 (5.93 ± 0.30) was significantly lower ($p < 0.05$) compared to NC, VC and ST groups on the corresponding days. In contrast, serum glucose level of CE was not

https://doi.org/10.2147/DDDT.S489113

Table 8 Mean Value of Different Glucose Levels Such as FBG, OGTT and Serum Glucose of Five Experimental Groups: SC, NC, VC, ST and CE

Groups	FBG (mmol/L)		OGTT (mmol/L)		Serum Glucose (mmol/L)	
	B.A.I	A.A.I	A.A.I at 0 min	A.A.I at 120 min	Day 3	Day 9
SC	4.53 ± 0.13	4.43 ± 0.15[a]	4.60 ± 0.14[b]	4.35 ± 0.18[c]	5.77 ± 0.30[d]	5.93 ± 0.30[e]
NC	4.60 ± 0.15	13.88 ± 0.48	14.43 ± 0.48	15.75 ± 0.37	11.43 ± 1.42	14.93 ± 1.05
VC	4.31 ± 0.17	13.48 ± 0.39	13.80 ± 0.38	16.06 ± 0.38	12.00 ± 1.12	11.67 ± 1.56
ST	4.18 ± 0.13	13.63 ± 0.39	13.98 ± 0.41	15.19 ± 0.44	11.53 ± 1.63	13.83 ± 1.22
CE	4.18 ± 0.12	14.10 ± 0.30	14.50 ± 0.29	15.61 ± 0.28	10.13 ± 0.97	9.77 ± 1.26

Notes: Data for FBG and OGTT are given as mean ± S.E. for twelve animals in each group and Data for serum glucose are given as mean ± S.E. for six animals in each group. Statistically significant results are indicated as [a]$p < 0.0001$, SC versus NC, VC, ST and CE on the corresponding stage; [b]$p < 0.0001$, SC versus NC, VC, ST and CE on the corresponding time; [c]$p < 0.0001$, SC versus NC, VC, ST and CE on the corresponding time; [d]$p < 0.05$, SC versus NC, VC, and ST on the corresponding day and [e]$p < 0.05$, SC versus NC, VC, and ST on the corresponding day.

Abbreviations: FBG, fasting blood glucose; OGTT, oral glucose tolerance test; B.A.I, before alloxan induction; A.A.I, after alloxan induction.

significantly difference than SC on both days. Results of serum liver biomarkers (AST and ALT) and lipid profiles (TC and TG) were similar trend like serum glucose (Table S3). Morphological assessment of liver and pancreas tissues had been reflected similar results of serum studies (Figures S3 and S4). In this figure, the rats in the SC group had a normal liver architecture, with sinusoidal hepatocyte cards and a central vein in the lobule's center. The cells of the liver are organized in sheets such as the spokes of a wheel. The liver was entirely distorted when diabetes was induced owing to inflammation in the hepatocytes (Figure S3). In addition, normal pancreatic structure featuring normal Langerhans islets in the middle with whitish spherical and ovoid cells embedded in the exocrine region of the pancreas, whereas, shrinkage of islets on Langerhans with degeneration and necrosis of component cells, with heavily basophilic nuclei and karyolysis visible in the diabetic groups (Figure S4).

Discussion

Diabetes mellitus is a chronic disorder characterized by hyperglycemia, which delays wound healing. The use of phytochemicals has shown potential in improving wound healing in diabetic conditions.[35,36] Wound contraction is a crucial step in the healing process that ultimately leads to wound closure. Previous studies have reported on the tissue's capacity to heal itself and the angiogenesis process, considering the type and extent of tissue damage and the overall state of tissue health.[37] Evaluations of wound contraction and visual assessments serve as credible criteria for assessing macroscopic wound healing.[38] The current investigation at the macroscopic level supports of initial hypothesis. During the wound healing process, *C. zeylanicum* extract stimulates the surrounding cells, leading to an increase in cell production. These findings, observed from a macroscopic perspective, allowed us to conclude that cinnamon positively influences wound healing by promoting the proliferation of surrounding tissues during treatment. By day 3, after the inflammatory stage, wounds treated with *C. zeylanicum* showed superior healing progress compared to the other groups. This result strongly correlates with cinnamon's anti-inflammatory properties. However, the persistence of inflammation during the anti-inflammatory phase (days 3–6) may slow wound healing. The observed reduction in inflammation aligns with expected results, leading to less redness and swelling and accelerating the overall healing process. Studies have shown that shortly after stable clot formation, the injured tissue is quickly colonized by cells involved in the inflammatory response.[39] Inflammatory cells create an environment that encourages macrophage and neutrophil infiltration to eliminate necrotic tissue, debris, and microbial sources while secreting inflammatory mediators and growth factors that activate fibroblasts.[40] The wound begins to heal more quickly due to the plant extract's beneficial proliferative properties, which become more effective over time. *C. zeylanicum* reduces swelling, redness, and pain associated with wounds, speeding up the healing process. It was observed that non-diabetic rats exhibited faster healing than diabetic rats,

confirming our original hypothesis regarding the delayed healing associated with diabetes. Previous studies have described that diabetic-related wounds have reduced vascularity and capillary density due to impaired angiogenesis. Diabetes significantly delays wound closure, and chronic non-healing wounds are common.[7] The group treated with *C. zeylanicum* extract showed better and more efficient healing than the other three diabetic groups. The *C. zeylanicum* treated rats began to heal around day 10, whereas it took approximately 16 days for the standard treatment with povidone-iodine dressing to achieve complete healing. Antiseptics like povidone-iodine and hydrogen peroxide inhibit fibroblast migration and proliferation in a dose-dependent manner.[41] As a result, cell migration into the wound is delayed, early wound matrix development is reduced, collagen synthesis is impaired, fibroblast proliferation is hindered, and wound contraction is inhibited in the povidone-iodine dressing group.[42] The ointment base group did not exhibit any significant wound-healing activity, suggesting that the base used for ointment preparation does not play a significant role in wound healing.[33] Histopathological findings in wound healing, such as re-epithelization, fibroblast proliferation, collagen deposition, and granulation tissue formation, are key indicators of the wound contraction process. Collagen fibrils play a crucial role by providing the mechanical strength needed for tissue contraction and wound closure.[43] Myofibroblasts, specialized fibroblasts, are essential in this process, migrating to the wound site, proliferating, and synthesizing granulation tissue, with their activity peaking 8 to 10 days post-injury.[44]

Hydroxyproline, a key collagen component, serves as an important indicator of tissue repair and remodeling.[45] Present study showed that *C. zeylanicum* extract treated group exhibited a notably elevated hydroxyproline content outperforming the other groups. This enhancement in hydroxyproline levels in the plant treated group underscores the potential efficacy of this treatment in promoting collagen synthesis and supporting wound healing.[46] Interestingly, hydroxyproline content of rats treated with povidone-iodine demonstrated a lack of improvement in the healing process. This stagnation suggests that povidone-iodine, typically regarded as a standard treatment, may not be sufficient to stimulate collagen deposition in this diabetic wound model.[47]

Reactive oxygen species (ROS) significantly contribute to oxidative stress, which impairs wound healing by damaging cellular components and delaying the inflammatory response.[48] Inflammatory cells, such as neutrophils and macrophages, release ROS at wound sites, leading to collagen breakdown and chronic wounds.[49,50] Antioxidant enzymes like catalase and glutathione play a crucial role in mitigating oxidative damage, as their levels are significantly elevated in treated groups compared to controls during late-stage wound healing.[51] However, the effectiveness of antioxidants can vary, and excessive ROS production remains a challenge in chronic wound management.[52] Lowering malondialdehyde (MDA) levels in granulation tissue is vital for speeding up wound healing, as MDA serves as an indicator of oxidative stress and cellular damage.[53] Elevated MDA levels are associated with slower healing due to heightened lipid peroxidation and inflammation, which obstruct the repair processes. Research indicates that reducing MDA levels can enhance wound healing by strengthening antioxidant defenses and encouraging fibroblast growth and collagen production.[54] Current study showed a significant reduction in the plant extract treated rats indicating a better wound healing outcomes. Thus, integrating phyto-therapies may improve healing outcomes by addressing oxidative stress and promoting tissue regeneration.

Matrix metalloproteinase (MMP), often referred to as matrix metallopeptidases or matrixins, are zinc-containing endopeptidases that are dependent on calcium.[55] Other members of this family include astacins, serralysins, and adamalysins. The MMPs are members of the metzincin superfamily, which is a wider family of proteases. When combined, these enzymes have the ability to break down every type of extracellular matrix protein and also digest many bioactive compounds. They have been linked to chemokine/cytokine inactivation, the release of apoptotic ligands (such the FAS ligand), and the cleavage of cell surface receptors.[56] Additionally, it is believed that MMPs are important for cellular activities such angiogenesis, apoptosis, differentiation, migration (adhesion/dispersion), and host defense.[57] One of the previously stated elements is the proteolytic enzyme MMP, which is strongly produced during the healing process and whose action is to break down the extracellular matrix (ECM), which causes the healing process to be delayed.[58] Hence, the ECM is less broken down by blocking MMP activity, which speeds up the healing of wounds.

Several studies showed that MMPs were potential predictive markers for impaired wound closure in diabetic foot ulcers.[55,56,59] The mRNA expression of MMP9 is significantly upregulated in the wounds of diabetic patients. Inhibitors of MMP9 can decrease the level of the protein and thereby facilitate faster wound healing. The protein MMP-8 plays role

in remodeling the extracellular matrix and healing the wound.[60] A strategy to hunt agonists of MMP8 can yield fruitful results in treatment of diabetic wound closure. Studies found that the mRNA expression of MMP9 was significantly higher in diabetic foot ulcers, while the expression of its inhibitors, TIMP1 and TIMP2, was significantly lower compared to normal wounds.[61] This suggests that diabetes increases MMP protein levels in wound tissues while decreasing TIMP proteins, potentially contributing to poor wound healing.

Phytochemicals play a significant role in the wound healing process by interacting with MMPs, particularly MMP8 and MMP9 proteins by accelerating the wound closure process.[62] Molecular docking is a commonly employed method in structure-based drug design, aiming to predict the optimal arrangement of a small molecule within the binding site of another molecule.[63] By targeting MMP8 and MMP9 proteins, phytochemicals exhibit promising therapeutic potential in promoting efficient wound healing and tissue regeneration. The GC-MS analysis of the *C. zeylanicum* extract identified thirty-three phytochemicals with potential medicinal properties. A docking score of - 6.00 kcal/mol or higher is considered the standard for an effective drug.[64] Most of phytochemicals of *C. zeylanicum* in this study has showed potential binding affinity with proteins. Binding Affinity of xanthosine with MMP8 and Methylquinoline with MMP9 were highest among all phytochemicals. Numerous studies reported that xanthosine has several biological activities, including promoting the expansion of mammary stem cells, hepatic stem cells, and hair follicle stem cells.[65] It can aslo regulate hepatic glucose homeostasis via signaling cascade. It Inhibits gluconeogenesis, activates glycogenesis through AMPK/FoxO1/AKT/GSK3β pathway.[66] Quinoline derivatives, including methylquinoline, exhibit diverse biological activities such as antibacterial, antifungal, anticancer, anti-HIV, antimalarial, antitumor, and anti-inflammatory properties.[67] Hydrogen bonding and hydrophobic interactions are pivotal in enhancing the interaction between drugs and receptors. In this study, all chosen ligand molecules demonstrated considerable formation of hydrogen bonds and hydrophobic interactions within binding site of target molecules.[68] This study has also found the main two types of bonds; hydrogen bonds and hydrophobic bonds. The van der Waal bond has also been examined, but it is not presented for all drugs. Drug-likeness which is known as the Lipinski rule or rules of five considered a vital element of a drug for drug likeness properties including molecular weight (MW), estimated solubility (ESOL) class, GI absorption and membrane permeability.[69] Most of ligands have been followed the Lipinski rule of five. All phytochemicals have lower than 500 g/mol of weight and most of the compounds obey the rule in terms of hydrogen bond acceptor and donors. Moreover, PASS can enrich the understanding of pharmacological potentials and aid in advancing drug development initiatives.[70] In the study, xanthosine demonstrate notable biological activities, such as isopenicillin-N epimerase inhibitors and various antiviral properties, including effectiveness against picornaviruses and poxviruses. Additionally, the potential for immunostimulant activity is particularly promising.

Molecular dynamics (MD) simulation is an essential tool for investigating biomolecules, offering a deeper understanding of ligand-protein interactions in molecular docking studies.[71] It serves as a critical method for verifying the results of molecular docking by simulating the behavior of molecules over time, thus providing dynamic insights that static docking cannot offer.[72] In this study, MD simulations of MMP8 and MMP9 protein-ligand complexes over 100 nanoseconds reveal key insights into their stability and conformational behavior. The RMSD analysis indicates that both proteins undergo conformational changes but remain stable, with MMP8 stabilizing around 2.5 nm and MMP9 around 7.5 nm. The ligands, Xanthosine for MMP8 and Methylquinoline for MMP9, show lower RMSD values, suggesting stable binding throughout the simulation. This flexibility is crucial when evaluating the stability of protein-ligand interactions, as it can highlight regions of structural stability or instability throughout the simulation. Thus, consistent RMSD values suggest a stable protein-ligand complex, while significant fluctuations may indicate instability or conformational changes.[73]

RMSF analysis identifies flexible regions within the proteins, crucial for understanding ligand binding and protein dynamics.[74] Xanthosine interacts with MMP8 through hydrogen bonds and electrostatic interactions, while Methylquinoline forms a strong, consistent interaction with tyrosine-420 in MMP9. The interaction patterns, visualized through stacked bar charts, highlight the significance of specific residues in stabilizing the complexes via hydrogen bonds, hydrophobic interactions, and water bridges.[75] The RMSF analysis reveals alternating stable and flexible regions within the protein structure. Atom indices 6 and 9 exhibit the lowest RMSF values (2.0 Å), indicating greater rigidity, while indices 1, 5, and 11 show higher flexibility, with 11 being the most dynamic at 2.6 Å. The RMSF oscillates between

2.0 and 2.6 Å, highlighting a dynamic landscape where flexible regions may correspond to loops or unstructured domains, and stable regions are likely structural cores. This pattern provides valuable insights into the protein's structural stability and functional dynamics.

The top graph likely represents the percentage of Secondary Structure (SS) over time, where peaks indicate regions of consistent structure (eg, alpha-helices, beta-sheets) important for stability, and lower points suggest flexible or disordered regions (eg, loops, coils) potentially involved in interactions or conformational changes. The bottom graph likely shows the evolution of secondary structure elements (SSEs) along the protein sequence over time, with different colors representing specific SSEs (eg, helices, sheets). Peaks in a color indicate the presence of a particular SSE at a residue, while low points suggest its absence. These graphs collectively provide insights into the protein's structural dynamics, stability, and functional regions, with interpretations depending on the simulation's time scale and the protein's biological context.

The top graph highlights the overall stability of secondary structure (SS%) over time, with minor fluctuations suggesting local conformational adjustments while maintaining a stable structural core. In contrast, the bottom graph reveals specific regions of stable secondary structure elements (SSEs), such as helices or sheets, alongside dynamic regions showing frequent transitions between SSE types, indicating structural flexibility. Stable regions likely contribute to the protein's overall stability, while dynamic regions may be crucial for functional roles like ligand binding or conformational changes. This comparative analysis underscores the protein's balance between structural rigidity and plasticity, essential for its stability and dynamic functionality.

These findings are essential for guiding future drug design efforts targeting MMP8 and MMP9, emphasizing the importance of selecting ligands that effectively bind and stabilize these proteins.[76]

Conclusion

C. zeylanicum extract possesses significant wound healing properties in in diabetic rats. The optimized *C. zeylanicum* extract demonstrated superior efficacy, resulting in faster recovery compared to other groups. This suggests that *C. zeylanicum* may serve as a promising natural alternative for the treatment of diabetic wounds and potentially offers a novel therapeutic strategy for managing diabetic complications. Moreover, the identification of active phytochemicals through molecular docking studies has shed light on the mechanisms by which *C. zeylanicum* exerts its therapeutic effects, particularly through the modulation of matrix metalloproteinases-8 and 9. This study underscores the potential of natural products in the development of therapies for diabetic wounds and related complications. In addition, considering all the computational parameters in this experiment, it can be concluded that the phytochemicals derived from *C. zeylanicum* extract play a potential role in the wound healing process. Specifically, xanthosine induces the MMP-8 protein, contributing to the remodeling of the extracellular matrix, while methylquinoline decreases the MMP-9 protein level, thereby facilitating faster wound healing.

Ethics Statement

All procedures in this study was approved by the Research Ethics Committee of University of Asia Pacific and followed the laboratory animal guideline for ethical review of animal welfare (Ref. no. UAP/REC/2022/111). All databases utilized in this study are publicly accessible and contain data available for unrestricted reuse under open licenses. In accordance with the guidelines provided by the National Research Ethics Committee (NREC) of Bangladesh Medical Research Council (BMRC), as stated in their official document (https://bmrcbd.org/application_form/EthicalGuidelines.pdf), the utilization of legally obtained public data is exempt from ethical review. Consequently, the aspect of this research involving public databases was granted an ethics approval waiver by the Ethics Committee of University of Asia Pacific.

Acknowledgments

The authors are thankful to the University of Asia Pacific for providing resources for this research. The authors also thank to Mohammad Shahriar and AKM Moyeenul Huq for technical support.

Disclosure

The author reports no conflicts of interest in this work.

References

1. Burgess JL, Wyant WA, Abdo Abujamra B, Jozic I. Diabetic wound-healing science. *Medicina*. 2021;57(10). doi:10.3390/medicina57101072
2. Robson MC, Steed DL, Franz MG. Wound healing: biologic features and approaches to maximize healing trajectories. *Curr Probl Surg*. 2001;38 (2):72–140. doi:10.1067/msg.2001.111167
3. Bowers S, Franco E. Chronic wounds: evaluation and management. *Am Fam Physician*. 2020;101(3):159–166.
4. Fu J, Wang Z, Huang L, et al. Review of the botanical characteristics, phytochemistry, and pharmacology of Astragalus membranaceus (Huangqi). *Phytother Res*. 2014;28(9):1275–1283. doi:10.1002/ptr.5188
5. Mieczkowski M, Mrozikiewicz-Rakowska B, Kowara M, Kleibert M, C L. The problem of wound healing in diabetes-from molecular pathways to the design of an animal model. *Int J Mol Sci*. 2022;23(14). doi:10.3390/ijms23147930
6. Flynn K, Mahmoud NN, Sharifi S, Gould LJ, Mahmoudi M. Chronic wound healing models. *ACS Pharmacol Transl Sci* 2023;6(5):783–801. doi:10.1021/acsptsci.3c00030
7. Okonkwo UA, DiPietro LA. Diabetes and wound angiogenesis. *Int J Mol Sci*. 2017;18(7):1419. doi:10.3390/ijms18071419
8. Wang X, Yuan CX, Xu B, Yu Z. Diabetic foot ulcers: classification, risk factors and management. *World J Diab*. 2022;13(12):1049–1065. doi:10.4239/wjd.v13.i12.1049
9. Jones RE, Foster DS, Longaker MT. Management of chronic wounds-2018. *JAMA*. 2018;320(14):1481–1482. doi:10.1001/jama.2018.12426
10. Jiang X, Zeng YE, Li C, Wang K, Yu DG. Enhancing diabetic wound healing: advances in electrospun scaffolds from pathogenesis to therapeutic applications. *Front Bioeng Biotechnol*. 2024;12:1354286. doi:10.3389/fbioe.2024.1354286
11. Matijević T, Talapko J, Meštrović T, et al. Understanding the multifaceted etiopathogenesis of foot complications in individuals with diabetes. *World J Clin Cases*. 2023;11(8):1669–1683. doi:10.12998/wjcc.v11.i8.1669
12. Ranasinghe P, Pigera S, Premakumara GA, Galappaththy P, Constantine GR, Katulanda P. Medicinal properties of 'true' cinnamon (Cinnamomum zeylanicum): a systematic review. *BMC Complement Altern Med*. 2013;13:275. doi:10.1186/1472-6882-13-275
13. Sharifi-Rad J, Dey A, Koirala N, et al. Cinnamomum species: bridging phytochemistry knowledge, pharmacological properties and toxicological safety for health benefits. *Front Pharmacol*. 2021;12:600139 doi:10.3389/fphar.2021.600139.
14. Gruenwald J, Freder J, Armbruester N. Cinnamon and health. *Crit Rev Food Sci Nutr*. 2010;50(9):822–834. doi:10.1080/10408390902773052
15. Muhammad DRA, Dewettinck K. Cinnamon and its derivatives as potential ingredient in functional food—A review. *Int J Food Prop*. 2017;20 (sup2):2237–2263.
16. Rao PV, Gan SH. Cinnamon: a multifaceted medicinal plant. *Evid Based Complement Alternat Med*. 2014;2014:642942. doi:10.1155/2014/642942
17. Abeysekera WPKM, Arachchige SPG, Abeysekera WKSM, Ratnasooriya WD, M HMUI. Antioxidant and glycemic regulatory properties potential of different maturity stages of leaf of Ceylon Cinnamon (Cinnamomum zeylanicum Blume) in vitro. *Evid Based Complement Alternat Med*. 2019;2019:2693795. doi:10.1155/2019/2693795
18. El Atki Y, Aouam I, El Kamari F, et al. Antibacterial activity of cinnamon essential oils and their synergistic potential with antibiotics. *J Adv Pharm Technol Res*. 2019;10(2):63–67. doi:10.4103/japtr.JAPTR_366_18
19. Cheng DM, Kuhn P, Poulev A, Rojo LE, Lila MA, Raskin I. In vivo and in vitro antidiabetic effects of aqueous cinnamon extract and cinnamon polyphenol-enhanced food matrix. *Food Chem*. 2012;135(4):2994–3002. doi:10.1016/j.foodchem.2012.06.117
20. Qin B, Nagasaki M, Ren M, Bajotto G, Oshida Y, Sato Y. Cinnamon extract (traditional herb) potentiates in vivo insulin-regulated glucose utilization via enhancing insulin signaling in rats. *Diabet Res Clin Pract*. 2003;62(3):139–148. doi:10.1016/S0168-8227(03)00173-6
21. Agu PC, Afiukwa CA, Orji OU, et al. Molecular docking as a tool for the discovery of molecular targets of nutraceuticals in diseases management. *Sci Rep*. 2023;13(1):13398. doi:10.1038/s41598-023-40160-2
22. Noor F, Tahir Ul Qamar M, Ashfaq UA, Albutti A, Alwashmi ASS, Aljasir MA. Network pharmacology approach for medicinal plants: review and assessment. *Pharmaceuticals*. 2022;15(5):572. doi:10.3390/ph15050572
23. Anqi L, Shijun S. Molecular docking, network pharmacology and experimental verification to explore the mechanism of Wulongzhiyangwan in the treatment of pruritus. *Sci Rep*. 2023;13(1):361. doi:10.1038/s41598-023-27593-5
24. Piñero J, Bravo À, Queralt-Rosinach N, et al. DisGeNET: a comprehensive platform integrating information on human disease-associated genes and variants. *Nucleic Acids Res*. 2017;45(D1):D833–d9. doi:10.1093/nar/gkw943
25. Szklarczyk D, Franceschini A, Wyder S, et al. STRING v10: protein-protein interaction networks, integrated over the tree of life. *Nucleic Acids Res*. 2015;43(Database issue):D447–52. doi:10.1093/nar/gku1003
26. Kuleshov MV, Jones MR, Rouillard AD, et al. Enrichr: a comprehensive gene set enrichment analysis web server 2016 update. *Nucleic Acids Res*. 2016;44(W1):W90–7. doi:10.1093/nar/gkw377
27. Daina A, Michielin O, Zoete V. SwissADME: a free web tool to evaluate pharmacokinetics, drug-likeness and medicinal chemistry friendliness of small molecules. *Sci Rep*. 2017;7(1):42717. doi:10.1038/srep42717
28. Filimonov DA, Lagunin AA, Gloriozova TA, et al. Prediction of the biological activity spectra of organic compounds using the pass online web resource. *Chem Heterocycl Compd*. 2014;50(3):444–457. doi:10.1007/s10593-014-1496-1
29. Hospital A, Goñi JR, Orozco M, Gelpí JL. Molecular dynamics simulations: advances and applications. *Adv Appl Bioinfo Chem*. 2015;8:37–47. doi:10.2147/AABC.S70333
30. López-Blanco JR, Aliaga JI, Quintana-Ortí ES, Chacón P. iMODS: internal coordinates normal mode analysis server. *Nucleic Acids Res*. 2014;42 (W1):W271–W6. doi:10.1093/nar/gku339
31. Ahmad SU, Akter S, Ghose KK, Tahira RN, Nasreen W, Bhuiyan MA. Evaluation of wound healing, antioxidant and antimicrobial effects of Cinnamomum zeylanicum extract: in vivo and in vitro approaches. *Med Health*. 2025;20:1.
32. Banda M, Nyirenda J, Muzandu K, Sijumbila G, Mudenda S. Antihyperglycemic and antihyperlipidemic effects of aqueous extracts of Lannea edulis in Alloxan-induced diabetic rats. *Front Pharmacol*. 2018;9:1099. doi:10.3389/fphar.2018.01099

33. Ahmad SU, Binti Aladdin NA, Jamal JA, Shuid AN, Mohamed IN. Evaluation of wound-healing and antioxidant effects of Marantodes pumilum (Blume) Kuntze in an excision wound model. *Molecules*. 2021;26(1):228. doi:10.3390/molecules26010228
34. Fernandes CPM, Lopes TV, SdO C, et al. Comparing open wound measuring methods popularly used in experimental studies. *Brazil J Veterinary Res Animal Sci*. 2015;52(2):106–111. doi:10.11606/issn.1678-4456.v52i2p106-111
35. Dra LA, Sellami S, Rais H, et al. Antidiabetic potential of Caralluma europaea against alloxan-induced diabetes in mice. *Saudi J Biol Sci*. 2019;26 (6):1171–1178. doi:10.1016/j.sjbs.2018.05.028
36. Qinna NA, Badwan AA. Impact of streptozotocin on altering normal glucose homeostasis during insulin testing in diabetic rats compared to normoglycemic rats. *Drug Des Devel Ther*. 2015;9:2515–2525. doi:10.2147/DDDT.S79885
37. Priya KS, Arumugam G, Rathinam B, Wells A, Babu M. Celosia argentea Linn. leaf extract improves wound healing in a rat burn wound model. *Wound Repair Regen*. 2004;12(6):618–625. doi:10.1111/j.1067-1927.2004.12603.x
38. Gal P, Kilik R, Mokry M, et al. Simple method of open skin wound healing model in corticosteroid-treated and diabetic rats: standardization of semi-quantitative and quantitative histological assessments. *Veterinární med*. 2008;53(12):652–659. doi:10.17221/1973-VETMED
39. Mohd Zaid NA, Sekar M, Bonam SR, et al. Promising natural products in new drug design, development, and therapy for skin disorders: an overview of scientific evidence and understanding their mechanism of action. *Drug Des Devel Ther*. 2023;16(null):23–66. doi:10.2147/DDDT.S326332
40. Henry G, Garner WL. Inflammatory mediators in wound healing. *Surg Clin North Ame*. 2003;83(3):483–507. doi:10.1016/S0039-6109(02)00200-1
41. Thomas GW, Rael LT, Bar-Or R, et al. Mechanisms of delayed wound healing by commonly used antiseptics. *J Trauma*. 2009;66(1):82–90. doi:10.1097/TA.0b013e31818b146d
42. Guo S, Dipietro LA. Factors affecting wound healing. *J Dental Res*. 2010;89(3):219–229. doi:10.1177/0022034509359125
43. Brauer E, Lippens E, Klein O, et al. Collagen fibrils mechanically contribute to tissue contraction in an in vitro wound healing scenario. *Adv Sci*. 2019;6(9):1801780. doi:10.1002/advs.201801780
44. Grinnell F. Fibroblasts, myofibroblasts, and wound contraction. *J Cell Biol*. 1994;124(4):401–404. doi:10.1083/jcb.124.4.401
45. Singh D, Rai V, Agrawal DK. Regulation of collagen I and collagen III in tissue injury and regeneration. *Cardiol Cardiovasc Med*. 2023;7(1):5–16. doi:10.26502/fccm.92920302
46. Schultz GS, Chin GA, Moldawer L, Diegelmann RF. Principles of Wound Healing. In: Fitridge R, Thompson M, editors. *Mechanisms of Vascular Disease: A Reference Book for Vascular Specialists*. Adelaide (AU): University of Adelaide Press © The Contributors; 2011:1.
47. Lin WY, Ma CY, Fang WC, et al. Dilute povidone-iodine solution soaking is ineffective in improving outcomes of necrotizing fasciitis caused by diabetic foot. *Annals Plastic Surg*. 2024;92(1S Suppl 1):S37–s40. doi:10.1097/SAP.0000000000003773
48. Maeso L, Antezana PE, Hvozda Arana AG, Evelson PA, Orive G, Desimone MF. Progress in the use of hydrogels for antioxidant delivery in skin wounds. *Pharmaceutics*. 2024;16(4):524. doi:10.3390/pharmaceutics16040524
49. Dospra M, Pavlou P, Papageorgiou S, Varvaresou A. Recent studies on the healing properties of eicosapentaenoic acid. *Appl Sci*. 2024;14(13):5884. doi:10.3390/app14135884
50. Accipe L, Abadie A, Neviere R, Bercion S. Antioxidant activities of natural compounds from Caribbean plants to enhance diabetic wound healing. *Antioxidants*. 2023;12(5):1079. doi:10.3390/antiox12051079
51. Balachandran A, Choi SB, Beata -M-M, et al. Antioxidant, wound healing potential and in silico assessment of naringin, eicosane and octacosane. *Molecules*. 2023;28(3):1043. doi:10.3390/molecules28031043
52. Lohana P, Suryaprawira A, Woods EL, et al. Role of enzymic antioxidants in mediating oxidative stress and contrasting wound healing capabilities in oral mucosal/skin fibroblasts and tissues. *Antioxidants*. 2023;12(7):1374. doi:10.3390/antiox12071374
53. Jabbar AAJ, Ahmed KAA, Abdulla MA, et al. Sinomenine accelerate wound healing in rats by augmentation of antioxidant, anti-inflammatory, immunuhistochemical pathways. *Heliyon*. 2024;10(1):e23581. doi:10.1016/j.heliyon.2023.e23581
54. Bagdas D, Gul NY, Topal A, et al. Pharmacologic overview of systemic chlorogenic acid therapy on experimental wound healing. *Naunyn-Schmiedeberg's Arch Pharmacol*. 2014;387(11):1101–1116. doi:10.1007/s00210-014-1034-9
55. Hariono M, Yuliani SH, Istyastono EP, Riswanto FDO, Adhipandito CF. Matrix metalloproteinase 9 (MMP9) in wound healing of diabetic foot ulcer: molecular target and structure-based drug design. *Wound Med*. 2018;22:1–13. doi:10.1016/j.wndm.2018.05.003
56. Liu Y, Min D, Bolton T, et al. Increased matrix metalloproteinase-9 predicts poor wound healing in diabetic foot ulcers. *Diab Care*. 2009;32 (1):117–119. doi:10.2337/dc08-0763
57. Quintero-Fabián S, Arreola R, Becerril-Villanueva E, et al. Role of matrix metalloproteinases in angiogenesis and cancer. *Front Oncol*. 2019;9:1370. doi:10.3389/fonc.2019.01370
58. Wang X, Khalil RA. Matrix metalloproteinases, vascular remodeling, and vascular disease. *Adv Pharmacol*. 2018;81:241–330. doi:10.1016/bs.apha.2017.08.002
59. Dai J, Shen J, Chai Y, Chen H. IL-1β impaired diabetic wound healing by regulating MMP-2 and MMP-9 through the p38 pathway. *Mediators Inflamm*. 2021;2021:6645766. doi:10.1155/2021/6645766
60. Chang M, Nguyen TT. Strategy for treatment of infected diabetic foot ulcers. *Acc Chem Res*. 2021;54(5):1080–1093. doi:10.1021/acs.accounts.0c00864
61. Ayuk SM, Abrahamse H, Houreld NN. The role of matrix metalloproteinases in diabetic wound healing in relation to photobiomodulation. *J Diab Res*. 2016;2016:2897656. doi:10.1155/2016/2897656
62. Cabral-Pacheco GA, Garza-Veloz I, Castruita-De la Rosa C, et al. The roles of matrix metalloproteinases and their inhibitors in human diseases. *Int J Mol Sci*. 2020;21(24):9739. doi:10.3390/ijms21249739
63. Gohlke H, Hendlich M, Klebe G. Knowledge-based scoring function to predict protein-ligand interactions. *J Mol Biol*. 2000;295(2):337–356. doi:10.1006/jmbi.1999.3371
64. Sarkar M, Nath A, Kumer A, et al. Synthesis, molecular docking screening, ADMET and dynamics studies of synthesized 4-(4-methoxyphenyl)-8-methyl-3,4,5,6,7,8-hexahydroquinazolin-2(1H)-one and quinazolinone derivatives. *J Mol Struct*. 2021;1244:130953. doi:10.1016/j.molstruc.2021.130953
65. Choudhary RK, Capuco AV. In vitro expansion of the mammary stem/progenitor cell population by xanthosine treatment. *BMC Cell Biol*. 2012;13:14. doi:10.1186/1471-2121-13-14

66. Ahmed SA, Sarma P, Barge SR, Swargiary D, Devi GS, Borah JC. Xanthosine, a purine glycoside mediates hepatic glucose homeostasis through inhibition of gluconeogenesis and activation of glycogenesis via regulating the AMPK/ FoxO1/AKT/GSK3β signaling cascade. *Chem Biol Interact* 2023;371:110347. doi:10.1016/j.cbi.2023.110347
67. Mohasin M, Zafer Alam M, Ullah Q, Ahmad A, Rahaman PF, Khan S A. A review on synthesis and biological applications of quinoline derivative as fused aromatic compounds. *Polycyclic Aromatic Compounds*. 2024; 44(9):6369–6398.
68. Davis AM, Teague SJ. Hydrogen bonding, hydrophobic interactions, and failure of the rigid receptor hypothesis. *Angewandte Chemie*. 1999;38 (6):736–749. doi:10.1002/(SICI)1521-3773(19990315)38:6<736::AID-ANIE736>3.0.CO;2-R
69. Ononamadu CJ, Ibrahim A. Molecular docking and prediction of ADME/drug-likeness properties of potentially active antidiabetic compounds isolated from aqueous-methanol extracts of Gymnema sylvestre and Combretum micranthum. *Biotechnologia*. 2021;102(1):85–99. doi:10.5114/bta.2021.103765
70. Ezike TC, Okpala US, Onoja UL, et al. Advances in drug delivery systems, challenges and future directions. *Heliyon*. 2023;9(6):e17488. doi:10.1016/j.heliyon.2023.e17488
71. Sasidharan S, Gosu V, Tripathi T, Saudagar P. Molecular Dynamics Simulation to Study Protein Conformation and Ligand Interaction. In: Saudagar P, Tripathi T, editors. *Protein Folding Dynamics and Stability: Experimental and Computational Methods*. Singapore: Springer Nature Singapore; 2023:107–127.
72. Zinnia MA, Khademul Islam A. Fenugreek steroidal saponins hinder osteoclastogenic bone resorption by targeting CSF-1R which diminishes the RANKL/OPG ratio. *Int J Biol Macromol*. 2021;186:351–364. doi:10.1016/j.ijbiomac.2021.06.197
73. Maruyama Y, Igarashi R, Ushiku Y, Mitsutake A. Analysis of protein folding simulation with moving root mean square deviation. *J Chem Inf Model*. 2023;63(5):1529–1541. doi:10.1021/acs.jcim.2c01444
74. Bornot A, Etchebest C, de Brevern AG. Predicting protein flexibility through the prediction of local structures. *Proteins*. 2011;79(3):839–852. doi:10.1002/prot.22922
75. Banerjee S, Baidya SK, Ghosh B, Jha T, Adhikari N. Exploration of structural alerts and fingerprints for novel anticancer therapeutics: a robust classification-QSAR dependent structural analysis of drug-like MMP-9 inhibitors. *SAR QSAR envir res*. 2023;34(4):299–319. doi:10.1080/1062936X.2023.2209737
76. Augoff K, Hryniewicz-Jankowska A, Tabola R, Stach K. MMP9: a tough target for targeted therapy for cancer. *Cancers*. 2022;14(7):1847. doi:10.3390/cancers14071847